Formulation methodologies based on Taylor expansion power and Fourier expansion series for the macro-element resolution scheme of enriched models for the stress analysis of adhesively bonded joints

Michel Salaün, Eric Paroissien, Sébastien Schwartz, Tuan-Long Vu, Valeria de Angelis, Maxime Luyat, Benjamin Ordonneau

Formulation methodologies based on Taylor expansion power and Fourier expansion series for the macro-element resolution scheme of enriched models for the stress analysis of adhesively bonded joints

Michel Salaün[a], Eric Paroissien[a,*], Sébastien Schwartz[a], Tuan-Long Vu[a], Valeria De Angelis[a], Maxime Luyat[a], Benjamin Ordonneau[a]

[a]*Institut Clément Ader, Université de Toulouse, ISAE-SUPAERO, INSA, IMT MINES ALBI, UTIII, CNRS, 3 Rue Caroline Aigle, Toulouse, 31400, France*

Abstract

In recent years, interest in adhesive bonding has grown as it can be considered an efficient solution in terms of strength-to-mass ratio when applied to lightweight structures or an interesting solution to complement conventional technologies. The study of bonded adhered joints is carried out using a technique based on the macro-element method (ME), the ME shape functions are modelled using Taylor expansion power and Fourier expansion series. The purpose of this work is to compare the stiffness matrix obtained first from the entire Taylor series and then with the entire Fourier series. The method has been developed so far for 1D-bar and 1D-beam kinematics frameworks.

Keywords: Macro-element, Fourier expansion series FES, Taylor expansion in power series TEPS, bonded joints

*Corresponding author
Email address: eric.paroissien@isae-supaero.fr (Eric Paroissien)

1. Introduction

The design of structures leads to the use of joining technologies. Adhesive bonding offers the ability of joining without damaging or modifying the physical characteristics of structural parts to be joined, eventually made in various materials, like metals or plastics. Moreover, the volume of adhesive materials, the specific mass of which is mainly slightly higher than the unity, required to transfer the loads, is very restricted. As a result, adhesive bonding can be regarded as an efficient solution in terms of strength-to-mass ratio when applied to lightweight structures or as an attractive solution to complement conventional technologies such as mechanical fastening in the frame of damage tolerant design approach for example.
The strength prediction of adhesive joints mainly involved an initial stress analysis which can be addressed by the Finite Element (FE) method [1, 2, 3, 4, 5, 6]. Nevertheless, to reduce the costs in terms of pre-processing, computational and post-processing times simplified stress analyses are attractive. As demonstrated in various review papers [7, 8, 9, 10, 6, 11], a large number of simplified stress analyses have been developed since the beginning of the 20th century [12]. A simplified stress analysis can be analytical or semi-analytical. An analytical stress analysis is fully led in close-form up to a ready-to-use equation. A semi-analytical stress analysis is partially led in close-form and requires a dedicated resolution computer program, based on more-or-less elementary numerical schemes, to provide the final result.
A widespread approach to simplify the stress analysis of bonded joints is to model the joints as two beams on elastic foundation. The adhesive layer is then seen as a bed of spring linking the kinematics of the adherends. The overlap composed by the beam and the adhesive layer is often referred to the sandwich zone. This approach is the one introduced in the fundamental analytical models of a single-lap bonded joint under membrane by Arnovljevic [12] and Volkersen [13], or under membrane and bending by Goland and Reissner [14]. However, depending on the nature of both adherends (similar or dissimilar), on the assumed constitutive model of materials (linear or non-linear), on the graduation of geometrical parameters, on the boundary conditions, the existence of a ready-to-use equation is not guaranteed. Indeed, even under linear analyses, the coupling of ordinary differential equations (ODEs) governing the system can be too severe. Semi-analytical approaches have then been developed to extend the application field of beams on elastic foundation modelling framework and to offer solutions where the analytical solution cannot be applied due to the enrichment or complexification of the set of hypotheses. The approach developed by Mortensen and Thomsen [15, 16, 17, 18] involves a particular resolution scheme based on the multi-segment integration method [19].
Another semi-analytical approach, called macro-element (ME) modelling, has been developed for some two decades by the authors of the present paper and their co-authors [11]. A ME is a 4-node brick representing for a bonded overlap so that it includes the assumed physics of the adhesive and adherends. This brick takes the shape of a stiffness matrix linking the nodal displacements with the nodal forces, which has to be formulated. The formulation of early ME stiffness matrices does not assume the shape of interpolation functions. Indeed, the interpolation functions take the shape of the solution of the system of governing ODEs, so that only one ME is needed to assess the solution at every abscissa along the overlap. The ME modelling is then able to support complicated configurations such as hybrid (bolted/bonded) joints [20, 21]. Associated with an iterative resolution scheme, non linear constitutive behaviors can be considered to simulate the progressive debonding of bonded

joints [22] or delamination of composite materials [23], similarly to cohesive zone modelling. In such a case, a discretization only along the overlap is required to locally update the material properties and then the ME stiffness matrices. To take advantage of the required discretization, a methodology of stiffness matrix formulation using the exponential of matrix has been developed [24]. This methodology does not required the shape of interpolations functions and significantly reduces the effort level in terms of mathematical pretreatment. The solution is then provided at the discretization nodes. This approach allows for an easily variation of initial simplifying hypotheses, such as the assumed beam model (Euler-Bernoulli or Timoshenko) or local equilibrium of adherends. In particular, it has been applied to the case where the adhesive properties are graduated along the overlap [24] or to the case of multilayered bonded joints [25]. To retrieve the ability to mode an entire overlap with only one ME while easily varying the initial set of simplifying hypotheses, two other approaches were developed. The first one makes use of the Jordan form to solve the system of coupled ODEs, the unknown of which is the vector of displacements and their derivatives [26]. The second one is based on the use of Taylor expansion power series (TEPS) [27, 28, 29], which has been applied on the graduation of adhesive properties and on the formulation of ME mass matrices. Following the previous path consisting in enriching the ME modelling, the objectives of this paper are to present the formulation methodologies based a new methodology based on TEPS, (ii) on Fourier expansion series (FES) and (iii) to validate and compare their convergence performance. Firslty, the formulation methodology of ME stiffness matrix based on FES is described under membrane (section 2) and under membrane plus bending (section 3), but more rapidly as it follows exactly the same way but with additional complexity due to the higher number of variables. This methodology has already been presented in [27] and [28] but in a different way. Furthermore, it is also given to introduce notations and to make easier the description of Fourier series methodology. The formulation based on FES is then validated and finally compared to the TEPS one in terms of convergence performance (section 4).

2. ME for the 1D Bar model

2.1. Assumptions and governing equations of 1D Bar model

Here is considered a single-lap joint structure, given in Figure 1. The first hypothesis is to consider this structure as monodimensional. The joint geometry is defined by the adherends thicknesses e_1 and e_2, respectively for the upper and lower one, while e_a is the adhesive thickness. Finally, L and b are half-length and width of adherends.
The model of single-lap joint is based on the following assumptions:

- both adherends are modelled as bars made of a homogeneous linear elastic material;
- the adhesive layer is modelled as an infinite number of shear springs linking the upper and lower adherends;
- the adhesive thickness is constant along the overlap;
- the adhesive stress is constant in the adhesive thickness.

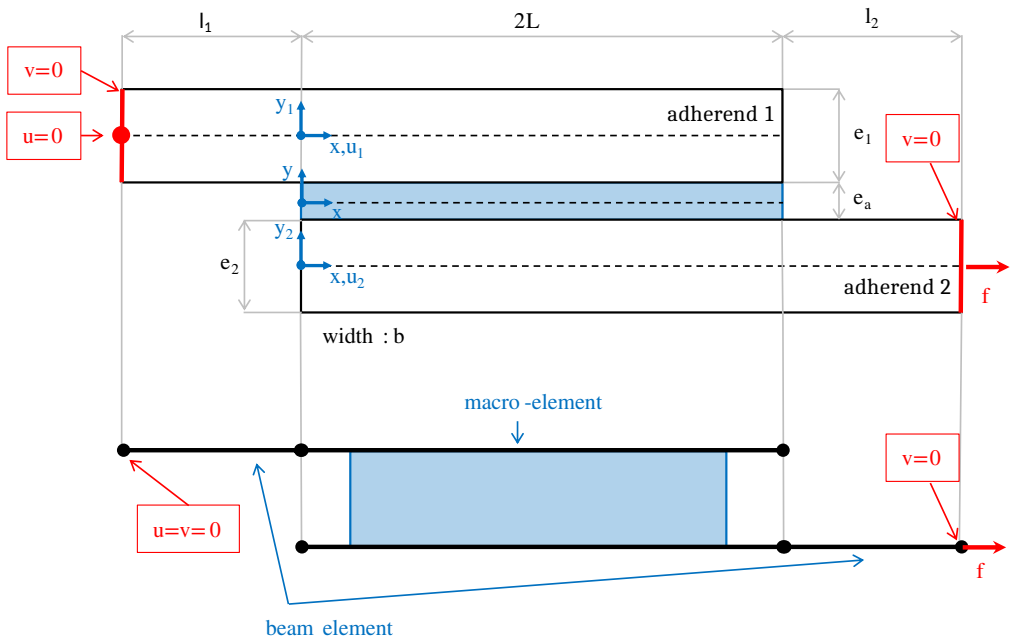

Figure 1: Simply supported single-lap involving the geometrical parameters, boundary conditions and in-plane loading.

The same equilibrium as Volkersen's [13] is used here (see Fig. 2). For both adherends, it leads to

$$\frac{dN_i(x)}{dx} = (-1)^i b T(x) \quad , \quad i = 1, 2 \tag{1}$$

where N_i is the normal force of adherend i and T is the adhesive shear stress.

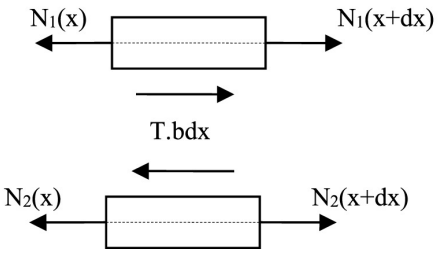

Figure 2: Free body diagram of infinitesimal pieces included between x and $x + dx$ of both adherends in the overlap region under 1D-bar kinematics. Subscript 1 (2) refers to the upper (lower) adherend.

The normal force in each adherend i is equal to:

$$N_i(x) = A_i \frac{du_i(x)}{dx} \quad , \quad i = 1, 2 \tag{2}$$

where $A_i = E_i e_i b$ is its membrane stiffness, E_i being its Young's Modulus. The normal displacement u_i is the displacement of the point on the neutral line of adherend i at abscissa x.

The expression of the shear stress in the adhesive layer depends on the expression of its shear modulus. If we consider a joint with homogeneous adhesive properties, the constitutive equation of the adhesive layer reads

$$T(x) \;=\; \frac{G_a}{e_a}\big(u_2(x)-u_1(x)\big) \quad , \tag{3}$$

where G_a is the shear modulus of the adhesive layer.
Introducing equations (2) and (3) in (1) leads to the following second order equations, expressed only in displacements

$$E_i e_i \frac{d^2u_i(x)}{dx^2} = (-1)^i \frac{G_a}{e_a}\big(u_2(x)-u_1(x)\big) \quad , \quad i=1,2 \quad . \tag{4}$$

Taylor series expansions on each displacement u_i were used to solve these equations in a previous paper [28]. Here, however, another method will be used, considering only the following set of first-order equations

$$\left\{ \begin{array}{lcl} \dfrac{dN_i(x)}{dx} &=& (-1)^i b \dfrac{G_a}{e_a}\big(u_2(x)-u_1(x)\big) \\ \\ \dfrac{du_i(x)}{dx} &=& \dfrac{1}{E_i e_i b} N_i(x) \qquad , \quad i=1,2 \quad . \end{array} \right. \tag{5}$$

2.2. Taylor expansion in power series (TEPS) for the 1D Bar model

For solving (5), the solution functions are searched as TEPS for any x between $-L$ and L, which means

$$\left\{ \begin{array}{lcl} u_i(x) &=& \displaystyle\sum_{n=0}^{+\infty} u_{i_n} x^n \\ \\ N_i(x) &=& \displaystyle\sum_{n=0}^{+\infty} N_{i_n} x^n \qquad , \quad i=1,2 \quad . \end{array} \right. \tag{6}$$

Then, the following variable change is made:

$$\xi \;=\; \frac{x}{L} \tag{7}$$

which means the solutions are functions of variable ξ, belonging to $]-1\ ,\ +1[$. Now, the unknown functions read

$$\left\{ \begin{array}{lcccccl} u_i(\xi) &=& \displaystyle\sum_{n=0}^{+\infty} u_{i_n}(L\xi)^n &=& \displaystyle\sum_{n=0}^{+\infty} u_{i_n} L^n \xi^n &\equiv& \displaystyle\sum_{n=0}^{+\infty} (u_i)_n \xi^n \\ \\ N_i(\xi) &=& \displaystyle\sum_{n=0}^{+\infty} N_{i_n}(L\xi)^n &=& \displaystyle\sum_{n=0}^{+\infty} N_{i_n} L^n \xi^n &\equiv& \displaystyle\sum_{n=0}^{+\infty} (N_i)_n \xi^n \qquad , \quad i=1,2 \end{array} \right. \tag{8}$$

where $(u_i)_n$ and $(N_i)_n$ are the adimensioned series coefficients. It should also be noted that this change of variable implies the following change in the derivative of any function, say φ

$$\frac{d\varphi(x)}{dx} \;=\; \frac{1}{L}\,\frac{d\varphi(\xi)}{d\xi} \quad . \tag{9}$$

The expressions of u_i and N_i are introduced in the equations (5). It follows, for all ξ and for all $i = 1, 2$

$$\left\{\begin{array}{rcl} \dfrac{1}{L}\;\displaystyle\sum_{n=1}^{+\infty} n\;(N_i)_n\xi^{n-1} & = & (-1)^i b\;\dfrac{G_a}{e_a}\;\left(\displaystyle\sum_{n=0}^{+\infty}(u_2)_n\xi^n - \sum_{n=0}^{+\infty}(u_1)_n\xi^n\right) \\ \dfrac{1}{L}\;\displaystyle\sum_{n=1}^{+\infty} n\;(u_i)_n\xi^{n-1} & = & \dfrac{1}{E_i e_i b}\;\displaystyle\sum_{n=0}^{+\infty}(N_i)_n\xi^n \qquad , \quad i = 1, 2 \end{array}\right. \tag{10}$$

which leads to the following recursive equations for all integer n

$$\left\{\begin{array}{rcl} \dfrac{n+1}{L}\;(N_i)_{n+1} \;-\; (-1)^i b\;\dfrac{G_a}{e_a}\;\big((u_2)_n - (u_1)_n\big) \;=\; 0 \\ \dfrac{n+1}{L}\;(u_i)_{n+1} \;-\; \dfrac{1}{E_i e_i b}\;(N_i)_n \;=\; 0 \qquad , \quad i = 1, 2 \quad . \end{array}\right. \tag{11}$$

To solve this set of equations, it's defined a truncation order, say N, which means all coefficients of order greater than N are set to 0. Therefore, the above relations are valid only for $0 \;\leq\; n \;\leq\; N-1$, which leads to a set of $4N$ equations, involving $4(N+1)$ unknowns ($(N+1)$ for each function u_1 , u_2 , N_1 and N_2). The vectors of unknowns is now presented, say C_{u_1} , C_{u_2} , C_{N_1} and C_{N_2} , defined as

$$C_{u_1} \;=\; \begin{bmatrix} (u_1)_0 \\ (u_1)_1 \\ \vdots \\ (u_1)_N \end{bmatrix} \qquad C_{u_2} = \begin{bmatrix} (u_2)_0 \\ (u_2)_1 \\ \vdots \\ (u_2)_N \end{bmatrix} \qquad C_{N_1} = \begin{bmatrix} (N_1)_0 \\ (N_1)_1 \\ \vdots \\ (N_1)_N \end{bmatrix} \qquad C_{N_2} = \begin{bmatrix} (N_2)_0 \\ (N_2)_1 \\ \vdots \\ (N_2)_N \end{bmatrix} \tag{12}$$

However, the objective is to build the stiffness matrix of the ME. The way to obtain it is the following. To complete the set of equations (11), the nodal displacement boundary conditions are added:

$$\left\{\begin{array}{rcccl} \widehat{u_1} & = & u_1(\xi = -1) & = & \displaystyle\sum_{n=0}^{N}(u_1)_n(-1)^n \\ \widehat{u_2} & = & u_2(\xi = -1) & = & \displaystyle\sum_{n=0}^{N}(u_2)_n(-1)^n \\ \widehat{u_3} & = & u_1(\xi = 1) & = & \displaystyle\sum_{n=0}^{N}(u_1)_n(1)^n \\ \widehat{u_4} & = & u_2(\xi = 1) & = & \displaystyle\sum_{n=0}^{N}(u_2)_n(1)^n \end{array}\right. \tag{13}$$

Then, the nodal force boundary conditions are written according to the sign convention defined Fig. 3:

$$\begin{cases} \widehat{N_1} &= -N_1(\xi=-1) &= -\sum_{n=0}^{N}(N_1)_n(-1)^n \\ \widehat{N_2} &= -N_2(\xi=-1) &= -\sum_{n=0}^{N}(N_2)_n(-1)^n \\ \widehat{N_3} &= N_1(\xi=1) &= \sum_{n=0}^{N}(N_1)_n(1)^n \\ \widehat{N_4} &= N_2(\xi=1) &= \sum_{n=0}^{N}(N_2)_n(1)^n \end{cases} \tag{14}$$

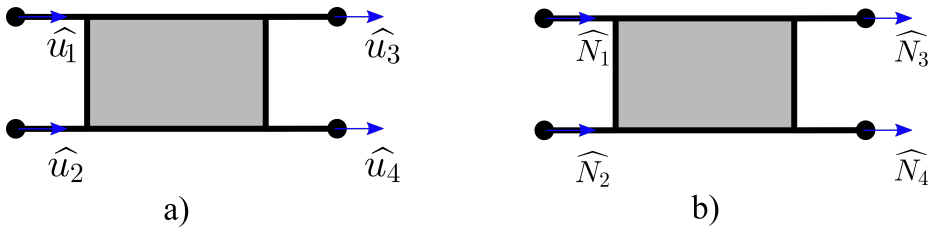

Figure 3: Nodal boundary condition diagram for 1D-bar kinematics. a) Nodal displacement b) Nodal forces including sign convention.

Finally, the 1D Bar ME stiffness matrix, say K_{ME}, is such that

$$K_{ME}\begin{bmatrix}\widehat{u_1}\\ \widehat{u_2}\\ \widehat{u_3}\\ \widehat{u_4}\end{bmatrix} = \begin{bmatrix}\widehat{N_1}\\ \widehat{N_2}\\ \widehat{N_3}\\ \widehat{N_4}\end{bmatrix} \tag{15}$$

and is obtained through the following way. First, gathering equations (11) and (13) leads to a square system of size $4(N+1)$, which formally reads

$$D_{ME}\begin{bmatrix}C_{u_1}\\ C_{u_2}\\ C_{N_1}\\ C_{N_2}\end{bmatrix} = \begin{bmatrix}[0]_{4N}\\ \widehat{u_1}\\ \widehat{u_2}\\ \widehat{u_3}\\ \widehat{u_4}\end{bmatrix} \tag{16}$$

or, conversely

$$\begin{bmatrix}C_{u_1}\\ C_{u_2}\\ C_{N_1}\\ C_{N_2}\end{bmatrix} = D_{ME}^{-1}\begin{bmatrix}[0]_{4N}\\ \widehat{u_1}\\ \widehat{u_2}\\ \widehat{u_3}\\ \widehat{u_4}\end{bmatrix} \tag{17}$$

which allows to compute C_{N_1} and C_{N_2} as functions of $\widehat{u_i}$

$$\begin{bmatrix} C_{N_1} \\ C_{N_2} \end{bmatrix} \;=\; \widehat{D_{ME}^{-1}} \; \begin{bmatrix} \widehat{u_1} \\ \widehat{u_2} \\ \widehat{u_3} \\ \widehat{u_4} \end{bmatrix} \tag{18}$$

where $\widehat{D_{ME}^{-1}}$ is the rectangular matrix built of the $2(N+1)$ last lines and 4 last columns of D_{ME}^{-1}. At last, with (14) which formally reads

$$\begin{bmatrix} \widehat{N_1} \\ \widehat{N_2} \\ \widehat{N_3} \\ \widehat{N_4} \end{bmatrix} \;=\; L_{ME} \; \begin{bmatrix} C_{N_1} \\ C_{N_2} \end{bmatrix} \tag{19}$$

where L_{ME} is a rectangular matrix of size 4 lines and $2(N+1)$ columns, is obtained

$$\begin{bmatrix} \widehat{N_1} \\ \widehat{N_2} \\ \widehat{N_3} \\ \widehat{N_4} \end{bmatrix} \;=\; L_{ME} \; \widehat{D_{ME}^{-1}} \; \begin{bmatrix} \widehat{u_1} \\ \widehat{u_2} \\ \widehat{u_3} \\ \widehat{u_4} \end{bmatrix} \tag{20}$$

which means the 1D Bar ME stiffness matrix reads

$$K_{ME} \;=\; L_{ME} \; \widehat{D_{ME}^{-1}} \quad . \tag{21}$$

Remark. The change of variable (7) is introduced because the calculations leading to the matrix K_{ME} are numerically more stable (see [30]).

2.3. Fourier series expansion (FSE) for the 1D Bar model

• **Preliminary remarks on FSE** (see [31] for example)
Now, for solving (5), the solution functions are searched as Fourier series for any x between $-L$ and L, which means the unknown functions are considered as $2L$ periodic functions. However, it is well known the Fourier series convergence is poor at a discontinuity point (Gibbs phenomenon), which is the case at the extremities of the joint as far as there is no reason the displacements nor the stresses will be equal there. For example, for u_1 displacement, one has

$$\widehat{u_1} \;=\; u_1(x=-L) \;\neq\; u_1(x=+L) \;=\; \widehat{u_3} \quad . \tag{22}$$

So, to recover good convergence properties, all the equations just mentioned must become continuous. To do this, we proceed as follows, considering for example a general $2L$ periodic function say φ which is assumed to be continuous inside the interval $]-L\ ,\ +L[$, but such that $\varphi(-L) \;\neq\; \varphi(+L)$. A new function called *Tildevarphi* is then introduced as

$$\tilde{\varphi}(x) \;=\; \varphi(x) \;-\; \frac{\varphi(+L) \;-\; \varphi(-L)}{2L} \; x \quad . \tag{23}$$

It is easy to check

$$\tilde{\varphi}(-L) \;=\; \tilde{\varphi}(+L) \;=\; \frac{\varphi(+L) \;+\; \varphi(-L)}{2} \quad , \tag{24}$$

which means $\tilde{\varphi}$ is $2L$ periodic function which is continuous on all $\mathbb{R}$. Then, the Fourier series of $\tilde{\varphi}$ uniformly converges towards $\tilde{\varphi}$ everywhere and may be derived term by term (Dirichlet-Jordan theorem). Thus one has

$$\tilde{\varphi}(x) \;=\; \frac{a_0(\tilde{\varphi})}{2} \;+\; \sum_{n=1}^{+\infty} \Big(a_n(\tilde{\varphi}) \;\cos\frac{n\pi x}{L} \;+\; b_n(\tilde{\varphi}) \;\sin\frac{n\pi x}{L} \Big) \quad , \tag{25}$$

for all x in $\mathbb{R}$, coefficients $a_n(\tilde{\varphi})$ and $b_n(\tilde{\varphi})$ being given by

$$\left\{ \begin{array}{rcl} a_n(\tilde{\varphi}) & = & \dfrac{1}{L} \displaystyle\int_{-L}^{+L} \tilde{\varphi}(x) \;\cos\frac{n\pi x}{L} \; dx \quad , \quad n \;\in\; \mathbb{N} \\ \\ b_n(\tilde{\varphi}) & = & \dfrac{1}{L} \displaystyle\int_{-L}^{+L} \tilde{\varphi}(x) \;\sin\frac{n\pi x}{L} \; dx \quad , \quad n \;\in\; \mathbb{N}^* \quad . \end{array} \right. \tag{26}$$

Finally, one obtains, for all x in $\mathbb{R}$

$$\begin{aligned} \frac{d\varphi(x)}{dx} \;&=\; \frac{d\tilde{\varphi}(x)}{dx} \;+\; \frac{\varphi(+L) \;-\; \varphi(-L)}{2L} \\ &=\; \sum_{n=1}^{+\infty} \Big(-a_n(\tilde{\varphi}) \;\frac{n\pi}{L} \;\sin\frac{n\pi x}{L} \;+\; b_n(\tilde{\varphi}) \;\frac{n\pi}{L} \;\cos\frac{n\pi x}{L} \Big) \;+\; \frac{\varphi(+L) \;-\; \varphi(-L)}{2L} \quad . \end{aligned} \tag{27}$$

• Application to the ME stiffness matrix computation

Consider (5). We introduce the continuous functions $Tildeu_i$ and $TildeN_i$ associated with u_i and N_i respectively via (23). Replacing these last functions by the continuous ones in (5) gives

$$\left\{ \begin{array}{rcl} \dfrac{d\tilde{N}_i(x)}{dx} \;+\; \dfrac{N_i(+L) \;-\; N_i(-L)}{2L} & = & (-1)^i b \dfrac{G_a}{e_a} \big(\tilde{u_2}(x) - \tilde{u_1}(x) \big) \;+\; (\Delta u)_i \; x \\ \\ \dfrac{d\tilde{u_i}(x)}{dx} \;+\; \dfrac{u_i(+L) \;-\; u_i(-L)}{2L} & = & \dfrac{1}{E_i e_i b} \tilde{N}_i(x) \;+\; (\Delta N)_i \; x \qquad , \quad i = 1, 2 \end{array} \right. \tag{28}$$

where it is set

$$\left\{ \begin{array}{rcl} (\Delta u)_i & = & (-1)^i b \dfrac{G_a}{e_a} \; \left(\dfrac{u_2(+L) \;-\; u_2(-L)}{2L} \;-\; \dfrac{u_1(+L) \;-\; u_1(-L)}{2L} \right) \\ \\ (\Delta N)_i & = & \dfrac{1}{E_i e_i b} \; \dfrac{N_i(+L) \;-\; N_i(-L)}{2L} \qquad , \quad i = 1, 2 \end{array} \right. \tag{29}$$

Now are introduced the Fourier series of $\tilde{u_i}$ and $\tilde{N_i}$, which read

$$\left\{\begin{array}{rcl} \tilde{u_i}(x) & = & \dfrac{a_0(\tilde{u_i})}{2} \ + \ \displaystyle\sum_{n=1}^{+\infty}\Big(a_n(\tilde{u_i}) \ \cos\frac{n\pi x}{L} \ + \ b_n(\tilde{u_i}) \ \sin\frac{n\pi x}{L}\Big) \\ \\ \tilde{N_i}(x) & = & \dfrac{a_0(\tilde{N_i})}{2} \ + \ \displaystyle\sum_{n=1}^{+\infty}\Big(a_n(\tilde{N_i}) \ \cos\frac{n\pi x}{L} \ + \ b_n(\tilde{N_i}) \ \sin\frac{n\pi x}{L}\Big) \qquad , \quad i=1,2 \end{array}\right. \tag{30}$$

and lead for $i = 1, 2$ to

$$\left\{\begin{array}{l} \displaystyle\sum_{n=1}^{+\infty}\Big(-a_n(\tilde{N_i}) \ \frac{n\pi}{L} \ \sin\frac{n\pi x}{L} \ + \ b_n(\tilde{N_i}) \ \frac{n\pi}{L} \ \cos\frac{n\pi x}{L}\Big) \ + \ \dfrac{N_i(+L) \ - \ N_i(-L)}{2L} \\ \quad = \ (-1)^i b\dfrac{G_a}{e_a}\left(\dfrac{a_0(\tilde{u_2})-a_0(\tilde{u_1})}{2}+\displaystyle\sum_{n=1}^{+\infty}\Big((a_n(\tilde{u_2})-a_n(\tilde{u_1}))\cos\frac{n\pi x}{L}+(b_n(\tilde{u_2})-b_n(\tilde{u_1}))\sin\frac{n\pi x}{L}\Big)\right) \\ \quad + \ (\Delta u)_i \ x \\ \\ \displaystyle\sum_{n=1}^{+\infty}\Big(-a_n(\tilde{u_i}) \ \frac{n\pi}{L} \ \sin\frac{n\pi x}{L} \ + \ b_n(\tilde{u_i}) \ \frac{n\pi}{L} \ \cos\frac{n\pi x}{L}\Big) \ + \ \dfrac{u_i(+L) \ - \ u_i(-L)}{2L} \\ \quad = \ \dfrac{1}{E_i e_i b}\left(\dfrac{a_0(\tilde{N_i})}{2} \ + \ \displaystyle\sum_{n=1}^{+\infty}\Big(a_n(\tilde{N_i}) \ \cos\frac{n\pi x}{L} \ + \ b_n(\tilde{N_i}) \ \sin\frac{n\pi x}{L}\Big)\right) \ + \ (\Delta N)_i \ x \end{array}\right. \tag{31}$$

To obtain the recursive equations for the integers n, the Fourier series of the function $varphi(x)$ $equiv$ x is calculated, giving

$$a_n(x) \ = \ 0 \ \ (n \ \in \ \mathbb{N}) \quad , \quad b_n(x) \ = \ \frac{1}{L}\int_{-L}^{+L} x \ \sin\frac{n\pi x}{L} \, dx \ = \ \frac{2L}{n\pi}\,(-1)^{n+1} \ \ (n \ \in \ \mathbb{N}^*) \quad . \tag{32}$$

Finally, each equation of the previous system leads respectively to 3 set of equations, corresponding to the constant term (namely a_0), the terms in $\cos\frac{n\pi x}{L}$ and the ones in $\sin\frac{n\pi x}{L}$. So the complete set of recursive equations reads for $i = 1, 2$ and $n \ \in \ \mathbb{N}^*$

$$\left\{\begin{array}{lcl}
(-1)^i b\ \dfrac{G_a}{e_a}\ \dfrac{a_0(\tilde{u_2}) - a_0(\tilde{u_1})}{2} & = & \dfrac{N_i(+L)\ -\ N_i(-L)}{2L} \\
b_n(\tilde{N_i})\ \dfrac{n\pi}{L}\ -\ (-1)^i b\ \dfrac{G_a}{e_a}(a_n(\tilde{u_2}) - a_n(\tilde{u_1})) & = & 0 \\
-a_n(\tilde{N_i})\ \dfrac{n\pi}{L}\ -\ (-1)^i b\ \dfrac{G_a}{e_a}\ (b_n(\tilde{u_2}) - b_n(\tilde{u_1})) & = & (\Delta u)_i\ \dfrac{2L}{n\pi}\ (-1)^{n+1} \\
\dfrac{1}{E_i e_i b}\ \dfrac{a_0(\tilde{N_i})}{2} & = & \dfrac{u_i(+L)\ -\ u_i(-L)}{2L} \\
b_n(\tilde{u_i})\ \dfrac{n\pi}{L}\ -\ \dfrac{1}{E_i e_i b} a_n(\tilde{N_i}) & = & 0 \\
-a_n(\tilde{u_i})\ \dfrac{n\pi}{L}\ -\ \dfrac{1}{E_i e_i b} b_n(\tilde{N_i}) & = & (\Delta N)_i\ \dfrac{2L}{n\pi}\ (-1)^{n+1}
\end{array}\right. \tag{33}$$

To solve this set of equations, as for TEPS, a truncation order is defined, say N, which means all coefficients of order greater than N are set to 0. Therefore, there are here $(2N+1)$ unknowns for each Fourier series so a total number of $4(2N+1)$ unknowns. But, contrarily to TEPS, there are $4(2N+1)$ equations in (33), which means the same number as unknowns. However, there is some difficulties with the "first" equations of (33), as one has, by taking $i = 1$ and $i = 2$

$$b\ \frac{G_a}{e_a}\ \frac{a_0(\tilde{u_2}) - a_0(\tilde{u_1})}{2}\ =\ -\ \frac{N_1(+L)\ -\ N_1(-L)}{2L}\ =\ \frac{N_2(+L)\ -\ N_2(-L)}{2L}\quad , \tag{34}$$

First, $a_0(\tilde{u_2})$ and $a_0(\tilde{u_1})$ only appears in these relations and only through their difference, so they cannot be separated. Second, relation (34) creates a link between the stresses N_1 and N_2 at the extremities of the joint. Actually,the equation (1) can be written as follows

$$\frac{dN_1(x)}{dx}\ =\ -\,bT(x)\ =\ -\,\frac{dN_2(x)}{dx} \tag{35}$$

which leads to

$$\frac{d(N_1(x) + N_2(x))}{dx}\ =\ 0 \tag{36}$$

or else $N_1(x) + N_2(x)$ is constant along the joint. So one has

$$N_1(+L) + N_2(+L) = N_1(-L) + N_2(-L)\ \iff\ N_2(+L) - N_2(-L) = -(N_1(+L) + N_1(-L)) \tag{37}$$

and there is no contradiction in (34). But it means one equation in set (33) is lost and remains the problem to separate $a_0(\tilde{u_2})$ and $a_0(\tilde{u_1})$. A way to tackle this problem is to go back to the Fourier series (30) giving $\tilde{u_i}$. Moreover, there is

$$\tilde{u_i}(\pm L)\ =\ \frac{u_i(+L)\ +\ u_i(-L)}{2}\ =\ \frac{a_0(\tilde{u_i})}{2}\ +\ \sum_{n=1}^{+\infty}(-1)^n\ a_n(\tilde{u_i})\quad , \tag{38}$$

which allows to obtain directly $a_0(\tilde{u_1})$. It is why the set of recursive equations (33) becomes for $i = 1, 2$ and $n \in \mathbb{N}^*$

$$\left\{\begin{array}{lcl} \dfrac{a_0(\tilde{u_i})}{2} + \displaystyle\sum_{n\geq 1}(-1)^n\, a_n(\tilde{u_i}) & = & \dfrac{u_i(+L) + u_i(-L)}{2} \\ \\ b_n(\tilde{N_i})\,\dfrac{n\pi}{L} - (-1)^i b\,\dfrac{G_a}{e_a}(a_n(\tilde{u_2}) - a_n(\tilde{u_1})) & = & 0 \\ \\ -a_n(\tilde{N_i})\,\dfrac{n\pi}{L} - (-1)^i b\,\dfrac{G_a}{e_a}\,(b_n(\tilde{u_2}) - b_n(\tilde{u_1})) & = & (\Delta u)_i\,\dfrac{2L}{n\pi}\,(-1)^{n+1} \\ \\ \dfrac{1}{E_i e_i b}\,\dfrac{a_0(\tilde{N_i})}{2} & = & \dfrac{u_i(+L) - u_i(-L)}{2L} \\ \\ b_n(\tilde{u_i})\,\dfrac{n\pi}{L} - \dfrac{1}{E_i e_i b}a_n(\tilde{N_i}) & = & 0 \\ \\ -a_n(\tilde{u_i})\,\dfrac{n\pi}{L} - \dfrac{1}{E_i e_i b}b_n(\tilde{N_i}) & = & (\Delta N)_i\,\dfrac{2L}{n\pi}\,(-1)^{n+1} \end{array}\right. \tag{39}$$

It should be noted that, in the previous equations, the sum appearing in the first relations is done for any $n \in \mathbb{N}^*$ in the general case, but becomes a sum from $n = 1$ to N when the truncation is done.

In the following, it is described how the 1D Bar ME stiffness matrix K_{ME} (see (16)) is obtained in the case of the FSE approach. The following notations are recalled

$$\left\{\begin{array}{lcllcl} \widehat{u_1} & = & u_1(-L) & \widehat{N_1} & = & -N_1(-L) \\ \widehat{u_2} & = & u_2(-L) & \widehat{N_2} & = & -N_2(-L) \\ \widehat{u_3} & = & u_1(+L) & \widehat{N_3} & = & N_1(+L) \\ \widehat{u_4} & = & u_2(+L) & \widehat{N_4} & = & N_2(+L) \end{array}\right. \tag{40}$$

according to the sign convention defined Fig. 3. Then the vectors of unknowns, say C_{u_1} , C_{u_2} , C_{N_1} and C_{N_2} , are introduced

$$C_{u_1} = \begin{bmatrix} a_0(\tilde{u_1}) \\ a_1(\tilde{u_1}) \\ \vdots \\ a_N(\tilde{u_1}) \\ b_1(\tilde{u_1}) \\ b_2(\tilde{u_1}) \\ \vdots \\ b_N(\tilde{u_1}) \end{bmatrix} \quad C_{u_2} = \begin{bmatrix} a_0(\tilde{u_2}) \\ a_1(\tilde{u_2}) \\ \vdots \\ a_N(\tilde{u_2}) \\ b_1(\tilde{u_2}) \\ b_2(\tilde{u_2}) \\ \vdots \\ b_N(\tilde{u_2}) \end{bmatrix} \quad C_{N_1} = \begin{bmatrix} a_0(\tilde{N_1}) \\ a_1(\tilde{N_1}) \\ \vdots \\ a_N(\tilde{N_1}) \\ b_1(\tilde{N_1}) \\ b_2(\tilde{N_1}) \\ \vdots \\ b_N(\tilde{N_1}) \end{bmatrix} \quad C_{N_2} = \begin{bmatrix} a_0(\tilde{N_2}) \\ a_1(\tilde{N_2}) \\ \vdots \\ a_N(\tilde{N_2}) \\ b_1(\tilde{N_2}) \\ b_2(\tilde{N_2}) \\ \vdots \\ b_N(\tilde{N_2}) \end{bmatrix} \tag{41}$$

First, definition of $(\Delta N)_i$ given in (29) and relation (34) allow to replace the last equations

of (39) by

$$\begin{aligned} -a_n(\tilde{u_i})\ \frac{n\pi}{L}\ -\ \frac{1}{E_i e_i b} b_n(\tilde{N_i}) \ &=\ \frac{1}{E_i e_i b}\ \frac{N_i(+L)\ -\ N_i(-L)}{2L}\ \frac{2L}{n\pi}\ (-1)^{n+1} \\ &=\ \frac{1}{E_i e_i b}\ \left((-1)^i b\ \frac{G_a}{e_a}\ \frac{a_0(\tilde{u_2}) - a_0(\tilde{u_1})}{2} \right)\ \frac{2L}{n\pi}\ (-1)^{n+1} \end{aligned} \tag{42}$$

which equivalently reads

$$a_n(\tilde{u_i})\ \frac{n\pi}{L}\ +\ \frac{1}{E_i e_i b} b_n(\tilde{N_i})\ +\ \frac{1}{E_i e_i b}\ \left((-1)^i b\ \frac{G_a}{e_a}\ \frac{a_0(\tilde{u_2}) - a_0(\tilde{u_1})}{2} \right)\ \frac{2L}{n\pi}\ (-1)^{n+1}\ =\ 0 \tag{43}$$

With this new relations, the right-hand side of equations (39) only depends on numbers $\widehat{u_i}$ but not on numbers $\widehat{N_i}$. This new set of equations formally becomes

$$D_{ME}\ \begin{bmatrix} C_{u_1} \\ C_{u_2} \\ C_{N_1} \\ C_{N_2} \end{bmatrix}\ =\ U_{ME}\ \begin{bmatrix} \widehat{u_1} \\ \widehat{u_2} \\ \widehat{u_3} \\ \widehat{u_4} \end{bmatrix} \tag{44}$$

where D_{ME} is a square matrix of size $4(2N+1)$ and U_{ME} is a rectangular matrix with $4(2N+1)$ lines and 4 columns. Hence one obtains

$$\begin{bmatrix} C_{u_1} \\ C_{u_2} \\ C_{N_1} \\ C_{N_2} \end{bmatrix}\ =\ D_{ME}^{-1}\ U_{ME}\ \begin{bmatrix} \widehat{u_1} \\ \widehat{u_2} \\ \widehat{u_3} \\ \widehat{u_4} \end{bmatrix} \tag{45}$$

Moreover, with the truncation, one gets

$$\frac{N_i(+L)\ +\ N_i(-L)}{2}\ =\ \tilde{N_i}(\pm L)\ =\ \frac{a_0(\tilde{N_i})}{2}\ +\ \sum_{n=1}^{N} (-1)^n\ a_n(\tilde{N_i}) \quad , \tag{46}$$

and (first equations of (33))

$$\frac{N_i(+L)\ -\ N_i(-L)}{2L}\ =\ (-1)^i b\ \frac{G_a}{e_a}\ \frac{a_0(\tilde{u_2}) - a_0(\tilde{u_1})}{2} \tag{47}$$

These relations equivalently read

$$\begin{cases} N_i(+L) \ &=\ \dfrac{a_0(\tilde{N_i})}{2}\ +\ \displaystyle\sum_{n=1}^{N} (-1)^n\ a_n(\tilde{N_i})\ +\ (-1)^i b L\ \frac{G_a}{e_a}\ \frac{a_0(\tilde{u_2}) - a_0(\tilde{u_1})}{2} \\ N_i(-L) \ &=\ \dfrac{a_0(\tilde{N_i})}{2}\ +\ \displaystyle\sum_{n=1}^{N} (-1)^n\ a_n(\tilde{N_i})\ -\ (-1)^i b L\ \frac{G_a}{e_a}\ \frac{a_0(\tilde{u_2}) - a_0(\tilde{u_1})}{2} \end{cases} \tag{48}$$

which formally becomes

$$\begin{bmatrix} \widehat{N_1} \\ \widehat{N_2} \\ \widehat{N_3} \\ \widehat{N_4} \end{bmatrix} = L_{ME} \begin{bmatrix} C_{u_1} \\ C_{u_2} \\ C_{N_1} \\ C_{N_2} \end{bmatrix} \tag{49}$$

where L_{ME} is a rectangular matrix of size 4 lines and $4(2N+1)$ columns. Finally, one attains

$$\begin{bmatrix} \widehat{N_1} \\ \widehat{N_2} \\ \widehat{N_3} \\ \widehat{N_4} \end{bmatrix} = L_{ME}\ D_{ME}^{-1}\ U_{ME} \begin{bmatrix} \widehat{u_1} \\ \widehat{u_2} \\ \widehat{u_3} \\ \widehat{u_4} \end{bmatrix} \tag{50}$$

which means the 1D Bar ME stiffness matrix reads

$$K_{ME} = L_{ME}\ D_{ME}^{-1}\ U_{ME} \quad . \tag{51}$$

3. ME for the 1D Beam model

3.1. Assumptions and governing equations of 1D Beam model

The development of the 1D Beam ME is based on the following assumptions:

- both adherends are modelled as linear elastic Euler-Bernoulli laminated beams;
- the adhesive layer is modelled as an infinite number of shear springs and peel springs linking the upper and lower adherends;
- the adhesive thickness is constant along the overlap;
- the adhesive stresses are constant in the adhesive thickness.

The equilibrium of the joint (see Fig. 4) comes from Goland and Reissner's analysis [14]. The system of equilibrium equations reads

$$\begin{cases} \dfrac{dN_i(x)}{dx} = (-1)^i b T(x) \\ \dfrac{dV_i(x)}{dx} = (-1)^{i+1} b S(x) \qquad\qquad i = 1,2 \\ \dfrac{dM_i(x)}{dx} = -V_i - \dfrac{be_i}{2} T(x) \end{cases} \tag{52}$$

where, for each adherend i, N_i is the normal force, V_i the shear force and M_i the bending moment at abscissa x. T is the adhesive shear stress and S the adhesive peel stress of the adhesive layer.Finally, it should be noted that b is the overlap width and e_i is the thickness of the adherent i.

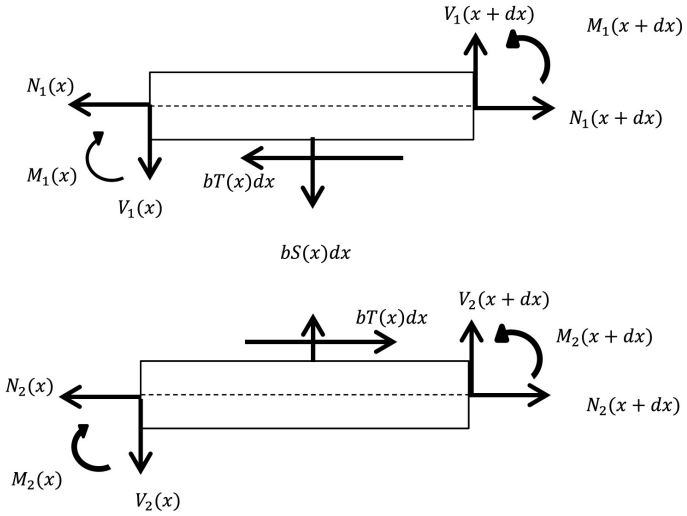

Figure 4: Free body diagram of infinitesimal pieces included between x and x + dx of both adherends in the overlap region under 1D-beam kinematics. Subscript 1 (2) refers to the upper (lower) adherend.

The constitutive equations of the adherends are

$$\begin{cases} N_i(x) &= A_i \dfrac{du_i(x)}{dx} - B_i \dfrac{d\theta_i(x)}{dx} \\ M_i(x) &= -B_i \dfrac{du_i(x)}{dx} + D_i \dfrac{d\theta_i(x)}{dx} \qquad i = 1,2 \\ \theta_i(x) &= \dfrac{dv_i(x)}{dx} \end{cases} \tag{53}$$

where, for each adherend i, A_i is the membrane stiffness, B_i the coupling membrane-bending stiffness and D_i the bending stiffness; Moreover, u_i is the displacement in the x-direction, v_i the normal deflection and θ_i the bending angle.
In the case of a homogeneous adhesive macro-element, the constitutive equations of the adhesive layer are

$$\begin{cases} T(x) &= \dfrac{G_a}{e_a} \left(u_2(x) - u_1(x) - \dfrac{e_2}{2}\theta_2(x) - \dfrac{e_1}{2}\theta_1(x) \right) \\ S(x) &= \dfrac{E_a}{e_a} \left(v_1(x) - v_2(x) \right) \end{cases} \tag{54}$$

where G_a is the shear modulus of the adhesive layer and E_a its adhesive peel modulus, which is the parameter characterising its transverse tensile behaviour. The variable e_a is redefined as the adhesive thickness.
Now, it is possible to replace in equation (52) the expressions of T and S given in (54), and those of N_i, M_i and θ_i given in (53) to obtain a differential system expressed only with respect to the u_i and v_i and their derivatives (up to the order 3 for u_i and 4 for v_i). It is the

way it is chosen in [28], where TEPS on each displacement u_i and v_i were used to solve these equations. But here again, as for 1D Bar model, we use an alternative way, considering only the following first order set of equations

$$\left\{\begin{array}{rcl} \dfrac{dN_i(x)}{dx} &=& (-1)^i b\ \dfrac{G_a}{e_a}\ \left(u_2(x) - u_1(x) - \dfrac{e_2}{2}\theta_2(x) - \dfrac{e_1}{2}\theta_1(x)\right) \\ \dfrac{dV_i(x)}{dx} &=& (-1)^{i+1} b\ \dfrac{E_a}{e_a}\ (v_1(x) - v_2(x)) \\ \dfrac{dM_i(x)}{dx} &=& -V_i - \dfrac{be_i}{2}\ \dfrac{G_a}{e_a}\ \left(u_2(x) - u_1(x) - \dfrac{e_2}{2}\theta_2(x) - \dfrac{e_1}{2}\theta_1(x)\right) \\ \dfrac{du_i(x)}{dx} &=& \dfrac{D_i}{A_iD_i - B_i^2}\ N_i(x) + \dfrac{B_i}{A_iD_i - B_i^2}\ M_i(x) \\ \dfrac{d\theta_i(x)}{dx} &=& \dfrac{B_i}{A_iD_i - B_i^2}\ N_i(x) + \dfrac{A_i}{A_iD_i - B_i^2}\ M_i(x) \\ \dfrac{dv_i(x)}{dx} &=& \theta_i(x) \end{array}\right. \qquad i = 1, 2 \qquad (55)$$

Let us remark this supposes $A_iD_i - B_i^2 \neq 0$ which is a classical hypothesis on material properties.

3.2. Taylor expansion in power series for the 1D Beam model

To solve (55), it is continued as done in the in Section 2.2. After the same variable change (see (7)), the solution functions are searched as TEPS for in ξ

$$\left\{\begin{array}{rclcrcl} u_i(\xi) &=& \displaystyle\sum_{n=0}^{+\infty}(u_i)_n\xi^n & & N_i(\xi) &=& \displaystyle\sum_{n=0}^{+\infty}(N_i)_n\xi^n \\ v_i(\xi) &=& \displaystyle\sum_{n=0}^{+\infty}(v_i)_n\xi^n & & V_i(\xi) &=& \displaystyle\sum_{n=0}^{+\infty}(V_i)_n\xi^n \\ \theta_i(\xi) &=& \displaystyle\sum_{n=0}^{+\infty}(\theta_i)_n\xi^n & & M_i(\xi) &=& \displaystyle\sum_{n=0}^{+\infty}(M_i)_n\xi^n \end{array}\right. \qquad i = 1, 2 \qquad (56)$$

It means there are now 12 unknown functions.

After having introduced the above expressions in equations (55), the following recursive

equations are obtained for all integer n and for all $i = 1, 2$

$$\begin{cases} \dfrac{n+1}{L}\,(N_i)_{n+1} \;-\; (-1)^i b\,\dfrac{G_a}{e_a}\left((u_2)_n - (u_1)_n - \dfrac{e_2}{2}(\theta_2)_n - \dfrac{e_1}{2}(\theta_1)_n\right) \;=\; 0 \\ \dfrac{n+1}{L}\,(V_i)_{n+1} \;-\; (-1)^{i+1} b\,\dfrac{E_a}{e_a}\left((v_1)_n - (v_2)_n\right) \;=\; 0 \\ \dfrac{n+1}{L}\,(M_i)_{n+1} \;+\; (V_i)_n \;+\; \dfrac{be_i}{2}\,\dfrac{G_a}{e_a}\left((u_2)_n - (u_1)_n - \dfrac{e_2}{2}(\theta_2)_n - \dfrac{e_1}{2}(\theta_1)_n\right) \;=\; 0 \\ \dfrac{n+1}{L}\,(u_i)_{n+1} \;-\; \dfrac{D_i}{A_iD_i - B_i^2}\,(N_i)_n \;-\; \dfrac{B_i}{A_iD_i - B_i^2}\,(M_i)_n \;=\; 0 \\ \dfrac{n+1}{L}\,(\theta_i)_{n+1} \;-\; \dfrac{B_i}{A_iD_i - B_i^2}\,(N_i)_n \;-\; \dfrac{A_i}{A_iD_i - B_i^2}\,(M_i)_n \;=\; 0 \\ \dfrac{n+1}{L}\,(v_i)_{n+1} \;-\; (\theta_i)_n \;=\; 0 \end{cases} \tag{57}$$

To solve this set of equations, it is defined a truncation order, say N. Therefore, the above relations are valid only for $0 \;\le\; n \;\le\; N-1$, which leads to a set of $12N$ equations, involving $12(N+1)$ unknowns ($(N+1)$ for each function). At this point one introduces the vectors of unknowns defined for all $i = 1, 2$ as

$$C_{u_i} = \begin{bmatrix} (u_i)_0 \\ (u_i)_1 \\ \vdots \\ (u_i)_N \end{bmatrix} \; C_{v_i} = \begin{bmatrix} (v_i)_0 \\ (v_i)_1 \\ \vdots \\ (v_i)_N \end{bmatrix} \; C_{\theta_i} = \begin{bmatrix} (\theta_i)_0 \\ (\theta_i)_1 \\ \vdots \\ (\theta_i)_N \end{bmatrix} \; C_{N_i} = \begin{bmatrix} (N_i)_0 \\ (N_i)_1 \\ \vdots \\ (N_i)_N \end{bmatrix} \; C_{V_i} = \begin{bmatrix} (V_i)_0 \\ (V_i)_1 \\ \vdots \\ (V_i)_N \end{bmatrix} \; C_{M_i} = \begin{bmatrix} (M_i)_0 \\ (M_i)_1 \\ \vdots \\ (M_i)_N \end{bmatrix} \tag{58}$$

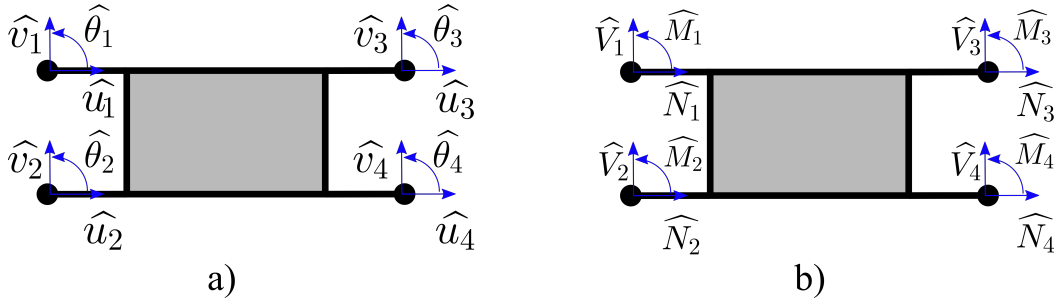

Figure 5: Nodal boundary condition diagram, 1D-beam kinematics. Nodal displacement (force) sign convention on the right (left) hand-side.

To complete the set of equations (57), the nodal displacement boundary conditions are added:

$$\begin{cases} \widehat{u}_1 \;=\; u_1(\xi=-1) & \widehat{v}_1 \;=\; v_1(\xi=-1) & \widehat{\theta}_1 \;=\; \theta_1(\xi=-1) \\ \widehat{u}_2 \;=\; u_2(\xi=-1) & \widehat{v}_2 \;=\; v_2(\xi=-1) & \widehat{\theta}_2 \;=\; \theta_2(\xi=-1) \\ \widehat{u}_3 \;=\; u_1(\xi=1) & \widehat{v}_3 \;=\; v_1(\xi=1) & \widehat{\theta}_3 \;=\; \theta_1(\xi=1) \\ \widehat{u}_4 \;=\; u_2(\xi=1) & \widehat{v}_4 \;=\; v_2(\xi=1) & \widehat{\theta}_4 \;=\; \theta_2(\xi=1) \end{cases} \tag{59}$$

Similarly, the nodal force boundary conditions are written according to the sign convention defined Fig. 5:

$$\left\{\begin{array}{lcllcllcl} \widehat{N_1} &=& -N_1(\xi=-1) & \widehat{V_1} &=& -V_1(\xi=-1) & \widehat{M_1} &=& -M_1(\xi=-1) \\ \widehat{N_2} &=& -N_2(\xi=-1) & \widehat{V_2} &=& -V_2(\xi=-1) & \widehat{M_2} &=& -M_2(\xi=-1) \\ \widehat{N_3} &=& N_1(\xi=1) & \widehat{V_3} &=& V_1(\xi=1) & \widehat{M_3} &=& M_1(\xi=1) \\ \widehat{N_4} &=& N_2(\xi=1) & \widehat{V_4} &=& V_2(\xi=1) & \widehat{M_4} &=& M_2(\xi=1) \end{array}\right. \tag{60}$$

Finally, the 1D Beam ME stiffness matrix, say K_{ME}, is the 12×12 matrix such that

$$K_{ME} \begin{bmatrix} \widehat{u_i} \\ \widehat{v_i} \\ \widehat{\theta_i} \end{bmatrix}_{i=1,4} = \begin{bmatrix} \widehat{N_i} \\ \widehat{V_i} \\ \widehat{M_i} \end{bmatrix}_{i=1,4} \tag{61}$$

It is obtained through the following way. First, gathering equations (57) and (59) leads to a square system of size $12(N+1)$, which formally reads

$$D_{ME} \begin{bmatrix} C_{u_i} \\ C_{v_i} \\ C_{\theta_i} \\ C_{N_i} \\ C_{V_i} \\ C_{M_i} \end{bmatrix}_{i=1,2} = \begin{bmatrix} [0]_{12N} \\ \begin{bmatrix} \widehat{u_i} \\ \widehat{v_i} \\ \widehat{\theta_i} \end{bmatrix}_{i=1,4} \end{bmatrix} \tag{62}$$

which allows to compute C_{N_i}, C_{V_i} and C_{M_i}

$$\begin{bmatrix} C_{N_i} \\ C_{V_i} \\ C_{M_i} \end{bmatrix}_{i=1,2} = \widehat{D_{ME}^{-1}} \begin{bmatrix} \widehat{u_i} \\ \widehat{v_i} \\ \widehat{\theta_i} \end{bmatrix}_{i=1,4} \tag{63}$$

where $\widehat{D_{ME}^{-1}}$ is the rectangular matrix built of the $6(N+1)$ last lines and 12 last columns of D_{ME}^{-1}. Finally, with (60) which formally reads

$$\begin{bmatrix} \widehat{N_i} \\ \widehat{V_i} \\ \widehat{M_i} \end{bmatrix}_{i=1,4} = L_{ME} \begin{bmatrix} C_{N_i} \\ C_{V_i} \\ C_{M_i} \end{bmatrix}_{i=1,2} \tag{64}$$

where L_{ME} is a rectangular matrix of size 12 lines and $6(N+1)$ columns, we obtain

$$\begin{bmatrix} \widehat{N_i} \\ \widehat{V_i} \\ \widehat{M_i} \end{bmatrix}_{i=1,4} = L_{ME} \widehat{D_{ME}^{-1}} \begin{bmatrix} \widehat{u_i} \\ \widehat{v_i} \\ \widehat{\theta_i} \end{bmatrix}_{i=1,4} \tag{65}$$

which means the 1D Beam ME stiffness matrix reads

$$K_{ME} = L_{ME} \widehat{D_{ME}^{-1}} \quad . \tag{66}$$

3.3. Fourier series expansion for the 1D Beam model

The procedure is the same as in 2.3. In (55) are introduced the continuous functions$\tilde{u_i}$, $\tilde{v_i}$, $\tilde{\theta}_i$, $\tilde{N}_i$, $\tilde{V}_i$ and $\tilde{M}_i$ associated respectively to u_i, v_i, θ_i, N_i, V_i and M_i through (23). It gives, for $i = 1, 2$

$$\left\{\begin{array}{rcl}
\dfrac{d\tilde{N}_i(x)}{dx} + \dfrac{N_i(+L) - N_i(-L)}{2L} &=& (-1)^i b\ \dfrac{G_a}{e_a}\ \left(\tilde{u_2}(x) - \tilde{u_1}(x) - \dfrac{e_2}{2}\tilde{\theta}_2(x) - \dfrac{e_1}{2}\tilde{\theta}_1(x)\right) + (\Delta u)_i\ x \\
\dfrac{d\tilde{V}_i(x)}{dx} + \dfrac{V_i(+L) - V_i(-L)}{2L} &=& (-1)^{i+1} b\ \dfrac{E_a}{e_a}\ (\tilde{v_1}(x) - \tilde{v_2}(x))\ +\ (\Delta v)_i\ x \\
\dfrac{d\tilde{M}_i(x)}{dx} + \dfrac{M_i(+L) - M_i(-L)}{2L} &=& -\tilde{V}_i(x) - \dfrac{be_i}{2}\ \dfrac{G_a}{e_a}\ \left(\tilde{u_2}(x) - \tilde{u_1}(x) - \dfrac{e_2}{2}\tilde{\theta}_2(x) - \dfrac{e_1}{2}\tilde{\theta}_1(x)\right) + (\Delta\theta)_i\ x \\
\dfrac{d\tilde{u_i}(x)}{dx} + \dfrac{u_i(+L) - u_i(-L)}{2L} &=& \dfrac{D_i}{A_iD_i - B_i^2}\ \tilde{N}_i(x) + \dfrac{B_i}{A_iD_i - B_i^2}\ \tilde{M}_i(x) + (\Delta N)_i\ x \\
\dfrac{d\tilde{\theta}_i(x)}{dx} + \dfrac{\theta_i(+L) - \theta_i(-L)}{2L} &=& \dfrac{B_i}{A_iD_i - B_i^2}\ \tilde{N}_i(x) + \dfrac{A_i}{A_iD_i - B_i^2}\ \tilde{M}_i(x) + (\Delta M)_i\ x \\
\dfrac{d\tilde{v_i}(x)}{dx} + \dfrac{v_i(+L) - v_i(-L)}{2L} &=& \tilde{\theta}_i(x) + \dfrac{\theta_i(+L) - \theta_i(-L)}{2L}\ x
\end{array}\right. \tag{67}$$

where we have set for $i = 1, 2$

$$\left\{\begin{array}{rcl}
(\Delta u)_i &=& (-1)^i b\dfrac{G_a}{e_a}\ \left(\dfrac{u_2(+L) - u_2(-L)}{2L} - \dfrac{u_1(+L) - u_1(-L)}{2L}\right. \\
&& \left. -\dfrac{e_2}{2}\dfrac{\theta_2(+L) - \theta_2(-L)}{2L} - \dfrac{e_1}{2}\dfrac{\theta_1(+L) - \theta_1(-L)}{2L}\right) \\
(\Delta v)_i &=& (-1)^{i+1} b\ \dfrac{E_a}{e_a}\ \left(\dfrac{v_1(+L) - v_1(-L)}{2L} - \dfrac{v_2(+L) - v_2(-L)}{2L}\right) \\
(\Delta\theta)_i &=& -\dfrac{V_i(+L) - V_i(-L)}{2L} - \dfrac{be_i}{2}\ \dfrac{G_a}{e_a}\ \left(\dfrac{u_2(+L) - u_2(-L)}{2L} - \dfrac{u_1(+L) - u_1(-L)}{2L}\right. \\
&& \left. -\dfrac{e_2}{2}\dfrac{\theta_2(+L) - \theta_2(-L)}{2L} - \dfrac{e_1}{2}\dfrac{\theta_1(+L) - \theta_1(-L)}{2L}\right) \\
(\Delta N)_i &=& \dfrac{D_i}{A_iD_i - B_i^2}\ \dfrac{N_i(+L) - N_i(-L)}{2L} + \dfrac{B_i}{A_iD_i - B_i^2}\ \dfrac{M_i(+L) - M_i(-L)}{2L} \\
(\Delta M)_i &=& \dfrac{B_i}{A_iD_i - B_i^2}\ \dfrac{N_i(+L) - N_i(-L)}{2L} + \dfrac{A_i}{A_iD_i - B_i^2}\ \dfrac{M_i(+L) - M_i(-L)}{2L}
\end{array}\right. \tag{68}$$

Then are introduced the Fourier series of the unknown functions, with the same notation convention as in equation (30), which means $a_n(\tilde{\psi})$ and $b_n(\tilde{\psi})$ are Fourier coefficient of any

function $\tilde{\psi}$. Using again the Fourier series decomposition of function $\varphi(x) \equiv x$, each equation of the previous system leads respectively to 3 sets of equations, corresponding to the constant term (namely a_0), the terms in $\cos\frac{n\pi x}{L}$ and the ones in $\sin\frac{n\pi x}{L}$. So the complete set of recursive equations reads • *Constant term* for $i = 1, 2$

$$\begin{cases} \dfrac{N_i(+L) - N_i(-L)}{2L} = (-1)^i b\ \dfrac{G_a}{e_a}\ \left(\dfrac{a_0(\tilde{u_2})}{2} - \dfrac{a_0(\tilde{u_1})}{2} - \dfrac{e_2}{2}\dfrac{a_0(\tilde{\theta_2})}{2} - \dfrac{e_1}{2}\dfrac{a_0(\tilde{\theta_1})}{2}\right) \\ \dfrac{V_i(+L) - V_i(-L)}{2L} = (-1)^{i+1} b\ \dfrac{E_a}{e_a}\ \left(\dfrac{a_0(\tilde{v_1})}{2} - \dfrac{a_0(\tilde{v_2})}{2}\right) \\ \dfrac{M_i(+L) - M_i(-L)}{2L} = -\dfrac{a_0(\tilde{V_i})}{2} - \dfrac{be_i}{2}\ \dfrac{G_a}{e_a}\ \left(\dfrac{a_0(\tilde{u_2})}{2} - \dfrac{a_0(\tilde{u_1})}{2} - \dfrac{e_2}{2}\dfrac{a_0(\tilde{\theta_2})}{2} - \dfrac{e_1}{2}\dfrac{a_0(\tilde{\theta_1})}{2}\right) \\ \dfrac{u_i(+L) - u_i(-L)}{2L} = \dfrac{D_i}{A_iD_i - B_i^2}\ \dfrac{a_0(\tilde{N_i})}{2} + \dfrac{B_i}{A_iD_i - B_i^2}\ \dfrac{a_0(\tilde{M_i})}{2} \\ \dfrac{\theta_i(+L) - \theta_i(-L)}{2L} = \dfrac{B_i}{A_iD_i - B_i^2}\ \dfrac{a_0(\tilde{N_i})}{2} + \dfrac{A_i}{A_iD_i - B_i^2}\ \dfrac{a_0(\tilde{M_i})}{2} \\ \dfrac{v_i(+L) - v_i(-L)}{2L} = \dfrac{a_0(\tilde{\theta_i})}{2} \end{cases} \tag{69}$$

• *Terms in* $\cos\frac{n\pi x}{L}$ for $i = 1, 2$ and $n \in \mathbb{N}^*$

$$\begin{cases} b_n(\tilde{N_i})\ \dfrac{n\pi}{L} = (-1)^i b\ \dfrac{G_a}{e_a}\ \left(a_n(\tilde{u_2}) - a_n(\tilde{u_1}) - \dfrac{e_2}{2}a_n(\tilde{\theta_2}) - \dfrac{e_1}{2}a_n(\tilde{\theta_1})\right) \\ b_n(\tilde{V_i})\ \dfrac{n\pi}{L} = (-1)^{i+1} b\ \dfrac{E_a}{e_a}\ (a_n(\tilde{v_1}) - a_n(\tilde{v_2})) \\ b_n(\tilde{M_i})\ \dfrac{n\pi}{L} = -a_n(\tilde{V_i}) - \dfrac{be_i}{2}\ \dfrac{G_a}{e_a}\ \left(a_n(\tilde{u_2}) - a_n(\tilde{u_1}) - \dfrac{e_2}{2}a_n(\tilde{\theta_2}) - \dfrac{e_1}{2}a_n(\tilde{\theta_1})\right) \\ b_n(\tilde{u_i})\ \dfrac{n\pi}{L} = \dfrac{D_i}{A_iD_i - B_i^2}\ a_n(\tilde{N_i}) + \dfrac{B_i}{A_iD_i - B_i^2}\ a_n(\tilde{M_i}) \\ b_n(\tilde{\theta_i})\ \dfrac{n\pi}{L} = \dfrac{B_i}{A_iD_i - B_i^2}\ a_n(\tilde{N_i}) + \dfrac{A_i}{A_iD_i - B_i^2}\ a_n(\tilde{M_i}) \\ b_n(\tilde{v_i})\ \dfrac{n\pi}{L} = a_n(\tilde{\theta_i}) \end{cases} \tag{70}$$

- *Terms in* $\sin\frac{n\pi x}{L}$ for $i=1,2$ and $n \in \mathbb{N}^*$

$$\left\{\begin{array}{l}
-a_n(\tilde{N}_i)\dfrac{n\pi}{L} = (-1)^i b\ \dfrac{G_a}{e_a}\left(b_n(\tilde{u_2}) - b_n(\tilde{u_1}) - \dfrac{e_2}{2}b_n(\tilde{\theta_2}) - \dfrac{e_1}{2}b_n(\tilde{\theta_1})\right) + (\Delta u)_i\ \dfrac{2L}{n\pi}(-1)^{n+1} \\
-a_n(\tilde{V}_i)\dfrac{n\pi}{L} = (-1)^{i+1} b\ \dfrac{E_a}{e_a}\ (b_n(\tilde{v_1}) - b_n(\tilde{v_2}))\ +\ (\Delta v)_i\ \dfrac{2L}{n\pi}(-1)^{n+1} \\
-a_n(\tilde{M}_i)\dfrac{n\pi}{L} = -b_n(\tilde{V}_i) - \dfrac{be_i}{2}\ \dfrac{G_a}{e_a}\left(b_n(\tilde{u_2}) - b_n(\tilde{u_1}) - \dfrac{e_2}{2}b_n(\tilde{\theta_2}) - \dfrac{e_1}{2}b_n(\tilde{\theta_1})\right) + (\Delta\theta)_i\ \dfrac{2L}{n\pi}(-1)^{n+1} \\
-a_n(\tilde{u_i})\dfrac{n\pi}{L} = \dfrac{D_i}{A_iD_i - B_i^2}\ b_n(\tilde{N}_i) + \dfrac{B_i}{A_iD_i - B_i^2}\ b_n(\tilde{M}_i) + (\Delta N)_i\ \dfrac{2L}{n\pi}(-1)^{n+1} \\
-a_n(\tilde{\theta_i})\dfrac{n\pi}{L} = \dfrac{B_i}{A_iD_i - B_i^2}\ b_n(\tilde{N}_i) + \dfrac{A_i}{A_iD_i - B_i^2}\ b_n(\tilde{M}_i) + (\Delta M)_i\ \dfrac{2L}{n\pi}(-1)^{n+1} \\
-a_n(\tilde{v_i})\dfrac{n\pi}{L} = b_n(\tilde{\theta_i}) + \dfrac{\theta_i(+L) - \theta_i(-L)}{2L}\ \dfrac{2L}{n\pi}(-1)^{n+1}
\end{array}\right. \tag{71}$$

Following Section 2.3, to solve this set of equations, a truncation order is defined, say N. Therefore, there are here $(2N+1)$ unknowns for each Fourier series so a total number of $12(2N+1)$ unknowns. As previously, it is observed that the number of equations (69)-(70)-(71) is equal to $12(2N+1)$ equations which is equal to the number of unknowns. But here also, there are exactly the some difficulties than in Section 2.3. More precisely, in the set (69), $a_0(\tilde{u_2})$ and $a_0(\tilde{u_1})$ only appears in expression $a_0(\tilde{u_2})\ -\ a_0(\tilde{u_1})$, like $a_0(\tilde{v_1})$ and $a_0(\tilde{v_2})$ through $a_0(\tilde{v_1})\ -\ a_0(\tilde{v_2})$. The consequences of these stress relations are not discussed as in Section 2.3 but is directly studied the solution proposed previously, which consists in going back to the truncated Fourier series giving $\tilde{u_i}$ and $\tilde{v_i}$:

$$\left\{\begin{array}{rcccl}
\tilde{u_i}(\pm L) & = & \dfrac{u_i(+L)\ +\ u_i(-L)}{2} & = & \dfrac{a_0(\tilde{u_i})}{2}\ +\ \displaystyle\sum_{n=1}^{N}(-1)^n\ a_n(\tilde{u_i}) \\
\tilde{v_i}(\pm L) & = & \dfrac{v_i(+L)\ +\ v_i(-L)}{2} & = & \dfrac{a_0(\tilde{v_i})}{2}\ +\ \displaystyle\sum_{n=1}^{N}(-1)^n\ a_n(\tilde{v_i})
\end{array}\right. \tag{72}$$

which allows to obtain directly $a_0(\tilde{u_i})$ and $a_0(\tilde{v_i})$. Likewise for the variable $\tilde{\theta_i}$

$$\tilde{\theta_i}(\pm L) \ = \ \frac{\theta_i(+L)\ +\ \theta_i(-L)}{2} \ = \ \frac{a_0(\tilde{\theta_i})}{2}\ +\ \sum_{n=1}^{N}(-1)^n\ a_n(\tilde{\theta_i}) \tag{73}$$

These new relations are used to replace the three first ones of (69), which become

$$\left\{\begin{array}{rcl}
\dfrac{u_i(+L)\ +\ u_i(-L)}{2} & = & \dfrac{a_0(\tilde{u_i})}{2}\ +\ \displaystyle\sum_{n=1}^{N}(-1)^n\ a_n(\tilde{u_i}) \\[2ex]
\dfrac{v_i(+L)\ +\ v_i(-L)}{2} & = & \dfrac{a_0(\tilde{v_i})}{2}\ +\ \displaystyle\sum_{n=1}^{N}(-1)^n\ a_n(\tilde{v_i}) \\[2ex]
\dfrac{\theta_i(+L)\ +\ \theta_i(-L)}{2} & = & \dfrac{a_0(\tilde{\theta_i})}{2}\ +\ \displaystyle\sum_{n=1}^{N}(-1)^n\ a_n(\tilde{\theta_i}) \\[2ex]
\dfrac{u_i(+L)-u_i(-L)}{2L} & = & \dfrac{D_i}{A_iD_i-B_i^2}\ \dfrac{a_0(\tilde{N_i})}{2}+\dfrac{B_i}{A_iD_i-B_i^2}\ \dfrac{a_0(\tilde{M_i})}{2} \\[2ex]
\dfrac{\theta_i(+L)-\theta_i(-L)}{2L} & = & \dfrac{B_i}{A_iD_i-B_i^2}\ \dfrac{a_0(\tilde{N_i})}{2}+\dfrac{A_i}{A_iD_i-B_i^2}\ \dfrac{a_0(\tilde{M_i})}{2} \\[2ex]
\dfrac{v_i(+L)-v_i(-L)}{2L} & = & \dfrac{a_0(\tilde{\theta_i})}{2}
\end{array}\right. \tag{74}$$

Below is obtained the 1D ME beam stiffness matrix K_{ME}, defined by (61). The same notations are used for the nodal displacements (59) and for the nodal force (60) as in 3.2, the only difference being that $\xi = -1$ and $\xi = +1$ now become $x = -L$ and $x = +L$ respectively. Then, for each unknown function, generically noted ψ, the vector of unknowns reads

$$C_\psi\ =\ \begin{bmatrix} a_0(\tilde{\psi}) \\ a_1(\tilde{\psi}) \\ \vdots \\ a_N(\tilde{\psi}) \\ b_1(\tilde{\psi}) \\ b_2(\tilde{\psi}) \\ \vdots \\ b_N(\tilde{\psi}) \end{bmatrix} \tag{75}$$

It can be observed that equations (74) and (70) only involve Fourier coefficients unknowns and nodal displacement boundary conditions but not nodal forces. Those ones only appear in (71), and only through the terms $(\Delta\theta)_i$, which involves $\frac{V_i(+L)-V_i(-L)}{2L}$, $(\Delta N)_i$ and $(\Delta M)_i$ which involves $\frac{N_i(+L)-N_i(-L)}{2L}$ and $\frac{M_i(+L)-M_i(-L)}{2L}$ (see (68)). However, the three first relations of (69) allow to write these 3 terms as functions of the Fourier series unknowns. With this new relations, the system (74)-(70)-(71) may formally rewritten as a square linear system which unknowns are all the Fourier coefficients, the right-hand side depending only on nodal displacements but not on nodal forces. This new set of equations formally becomes

$$D_{ME}\ C\ =\ U_{ME}\ \widehat{U}\quad , \tag{76}$$

where D_{ME} is a square matrix of size $12(2N+1)$, C is the vector gathering the $12(2N+1)$ Fourier coefficients, U_{ME} is a rectangular matrix with $12(2N+1)$ lines and 12 columns and $\widehat{U}$ contains the 12 nodal displacements given in (59). Conversely, it becomes

$$C \;=\; D_{ME}^{-1}\, U_{ME}\, \widehat{U} \quad . \tag{77}$$

The last step is the following. With the truncation, one has

$$\left\{\begin{array}{rcccl} \dfrac{N_i(+L) \;+\; N_i(-L)}{2} & = & \tilde{N}_i(\pm L) & = & \dfrac{a_0(\tilde{N}_i)}{2} \;+\; \displaystyle\sum_{n=1}^{N}(-1)^n\, a_n(\tilde{N}_i) \\ \dfrac{M_i(+L) \;+\; M_i(-L)}{2} & = & \tilde{M}_i(\pm L) & = & \dfrac{a_0(\tilde{M}_i)}{2} \;+\; \displaystyle\sum_{n=1}^{N}(-1)^n\, a_n(\tilde{M}_i) \\ \dfrac{V_i(+L) \;+\; V_i(-L)}{2} & = & \tilde{V}_i(\pm L) & = & \dfrac{a_0(\tilde{V}_i)}{2} \;+\; \displaystyle\sum_{n=1}^{N}(-1)^n\, a_n(\tilde{V}_i) \end{array}\right. \tag{78}$$

The three first relations of (69) read

$$\left\{\begin{array}{l} \dfrac{N_i(+L)-N_i(-L)}{2L} = (-1)^i b\, \dfrac{G_a}{e_a}\, \left(\dfrac{a_0(\tilde{u_2})}{2} - \dfrac{a_0(\tilde{u_1})}{2} - \dfrac{e_2}{2}\dfrac{a_0(\tilde{\theta_2})}{2} - \dfrac{e_1}{2}\dfrac{a_0(\tilde{\theta_1})}{2} \right) \\ \dfrac{V_i(+L)-V_i(-L)}{2L} = (-1)^{i+1} b\, \dfrac{E_a}{e_a}\, \left(\dfrac{a_0(\tilde{v_1})}{2} - \dfrac{a_0(\tilde{v_2})}{2} \right) \\ \dfrac{M_i(+L)-M_i(-L)}{2L} = -\dfrac{a_0(\tilde{V_i})}{2} - \dfrac{be_i}{2}\, \dfrac{G_a}{e_a}\, \left(\dfrac{a_0(\tilde{u_2})}{2} - \dfrac{a_0(\tilde{u_1})}{2} - \dfrac{e_2}{2}\dfrac{a_0(\tilde{\theta_2})}{2} - \dfrac{e_1}{2}\dfrac{a_0(\tilde{\theta_1})}{2} \right) \end{array}\right. \tag{79}$$

By simple linear combinations, it is easy to express the vector of the 12 nodal forces, say $\widehat{N}$, as functions of all the Fourier coefficients, which formally becomes

$$\widehat{N} \;=\; L_{ME}\, C \;=\; L_{ME}\, D_{ME}^{-1}\, U_{ME}\, \widehat{U} \quad , \tag{80}$$

where L_{ME} is a rectangular matrix of size 12 lines and $12(2N+1)$ columns. Finally, is obtained the 1D Beam ME stiffness matrix

$$K_{ME} \;=\; L_{ME}\, D_{ME}^{-1}\, U_{ME} \quad . \tag{81}$$

4. Validation

4.1. Method

The formulation methodologies presented in section 2 and section 3 are implemented in Matlab codes which are supplementary materials of the present paper. The ME stiffness matrices based on expansion series (TEPS or FES) are dependent on the truncation order N.

The validation method consists then in assessing the convergence ME based-series stiffness matrices as function of N. The convergence is then expressed as function of N with respect to reference stiffness matrices, based on two cases for both 1D-bar and 1D-beam model: a balanced case and an unbalanced case. The geometrical parameters used are the same for both cases and are provided in Table 1. The material properties are given in Table 2. For both cases, the adhesive material parameters are the same. The unbalanced case differs from the balanced case by varying the Young's modulus of the upper adherend only.

L	b	e_1	e_2	e_a
$6,25$	25	2	2	$0,2$

Table 1: Geometrical parameters in mm

	E_1	E_2	G_a	E_a
Balanced case	70000	70000	800	2240
Unblanced case	210000			

Table 2: Material parameters in MPa

In the case of the 1D-bar ME with homogeneous properties, the closed-form expression for the ME stiffness matrix is known [32, 11]. It is then regarded as the reference 1D-bar ME stiffness matrix and is recalled here:

$$K_{ME} = \frac{1}{1+\chi}\frac{A_2}{2L}\begin{pmatrix} \frac{\omega}{\tanh\omega}+\frac{1}{\chi} & 1-\frac{\omega}{\tanh\omega} & -\frac{\omega}{\sinh\omega}-\frac{1}{\chi} & \frac{\omega}{\sinh\omega}-1 \\ 1-\frac{\omega}{\tanh\omega} & \frac{\omega}{\tanh\omega}+\chi & \frac{\omega}{\sinh\omega}-1 & -\frac{\omega}{\sinh\omega}-\chi \\ -\frac{\omega}{\sinh\omega}-\frac{1}{\chi} & \frac{\omega}{\sinh\omega}-1 & \frac{\omega}{\tanh\omega}+\frac{1}{\chi} & 1-\frac{\omega}{\tanh\omega} \\ \frac{\omega}{\sinh\omega}-1 & -\frac{\omega}{\sinh\omega}-\chi & 1-\frac{\omega}{\tanh\omega} & \frac{\omega}{\tanh\omega}+\chi \end{pmatrix} \tag{82}$$

where χ and ω are nondimensional parameters given by $\chi = \frac{A_2}{A_1}$ and $\omega = 2L\sqrt{\frac{G_a}{e_a}\frac{1+\chi}{e_2 E_2}}$. In the case of 1D-beam ME, the ME stiffness matrix components are not provided in closed-form due to the complexity of the mathematical treatment. When the properties are homogeneous, they can be deduced from algebraic manipulations without any approximations [20] using, for example, a method involving coupling matrices D_{ME} and L_{ME} [23, 11]. It is then regarded as the reference 1D-beam ME stiffness matrix and a Matlab code is available as supplementary material of the paper by Lachaud et al. [23].
The convergence is firstly assessed by a comparison components by components of the approximated ME stiffness matrices by expansion series with the reference one through the following error indicator:

$$error \;=\; \frac{\sum_{i=1}^{P}\sum_{j=1}^{P}|K_{ij}^{exact} \;-\; K_{ij}^{series}|}{\max_{ij}|K_{ij}^{exact}|} \tag{83}$$

where P is the total number of degrees of freedom: $P = 4$ ($P = 12$) for the 1D-bar (1D-beam) model.
A second convergence assessment is dedicated to the computed displacement jumps at the interface for the classical single-lap joint configuration. The displacement jumps are evaluated at both overlap ends where they are maximal. For simplicity, the boundary conditions are directly introduced at the four ME nodes by prescribing or loading degrees of freedom. This approach is like sandwich-type analyses of bonded joints. The prescription of degrees of freedom leads to an inversible structural stiffness matrix K_s while the loading of degrees of freedom leads to the feeding of a structural nodal force vector F_s. The minimization of the potential energy leads to the classical equation $F_s = K_s U_s$ where U_s is the structural nodal displacement vector. For the 1D-bar model, the degree of freedom of the left-side upper adherend node is prescribed ($\widehat{u_1} = 0$) while the force $F = 5$ kN is applied to the right-side lower adherend node: $\widehat{N_4} = F$. A 3×3 linear system has then to be solved. For the 1D-beam model, the 3 degrees of freedom of the left-side upper adherend are prescribed ($\widehat{u_1} = 0$, $\widehat{v_1} = 0$, $\widehat{\theta_1} = 0$) while the the right-side lower adherend node is loaded such as: $\widehat{N_4} = F$, $\widehat{V_4} = -V_0$ and $\widehat{M_4} = -M_0$. The values of V_0 and M_0 are chosen following the approach of Cheng et al. [33] to approximately consider the nonlinear geometrical effect due to eccentricity of the load path. They are then depending on F. For a balanced joint, it is indicated that the Cheng et al. approach reduces to the Goland and Reissner approach. The values of M_0 and V_0 are then given in Table 3 for the balanced and unbalanced cases. A 9×9 linear system has then to be solved for the 1D-beam model.

	V_0	M_0
Balanced case	231	3555
Unblanced case	297	3282

Table 3: Values of V_0 in N and M_0 in Nmm for both cases

For the 1D-bar model, the interface displacement jumps in shear δ_u of the in $x = -L$ and $x = +L$ are computed such us $\delta_u(-L) = \widehat{u_2} - \widehat{u_1}$ and $\delta_u(L) = \widehat{u_4} - \widehat{u_3}$. For the 1D-beam model, the interface displacement jumps in shear δ_u and in peel δ_v of the in $x = -L$ and $x = +L$ are computed such us $\delta_u(-L) = \widehat{u_2} - \widehat{u_1} - \frac{1}{2}e_2\widehat{\theta_2} - \frac{1}{2}e_1\widehat{\theta_1}$, $\delta_u(L) = \widehat{u_4} - \widehat{u_3} - \frac{1}{2}e_2\widehat{\theta_4} - \frac{1}{2}e_1\widehat{\theta_3}$, $\delta_v(-L) = \widehat{v_1} - \widehat{v_2}$ and $\delta_v(L) = \widehat{v_3} - \widehat{v_4}$. The absolute values of the relative difference with the displacements jumps computed from the related reference ME stiffness matrix are then computed.

4.2. Results for FES formulation

4.2.1. 1D-Bar model

For both balanced and unbalanced cases, as a function of the truncation order N, the variation of the error indicator as well as the absolute values of relative difference in interface displacement jumps in shear δ_u in $x = -L$ and $x = +L$ are provided in Fig. 6 and Fig. 7 respectively. For the balanced case, the absolute values of relative difference in displacement jumps are the same in $x = -L$ and in $x = +L$ for every truncation number N. It is shown that the error as well as the relative difference are decreasing functions of increasing

truncation number N. The more N is elevated, the more the approximated stiffness matrix components and the interface displacements jumps tends to the reference ones. Errors and relative differences around 1% are obtained for N=100. In addition, best fitting curves are provided in the shape of power law. A convergence for the error indicator and displacement jumps in shear in $\frac{1}{N}$ is then measured.

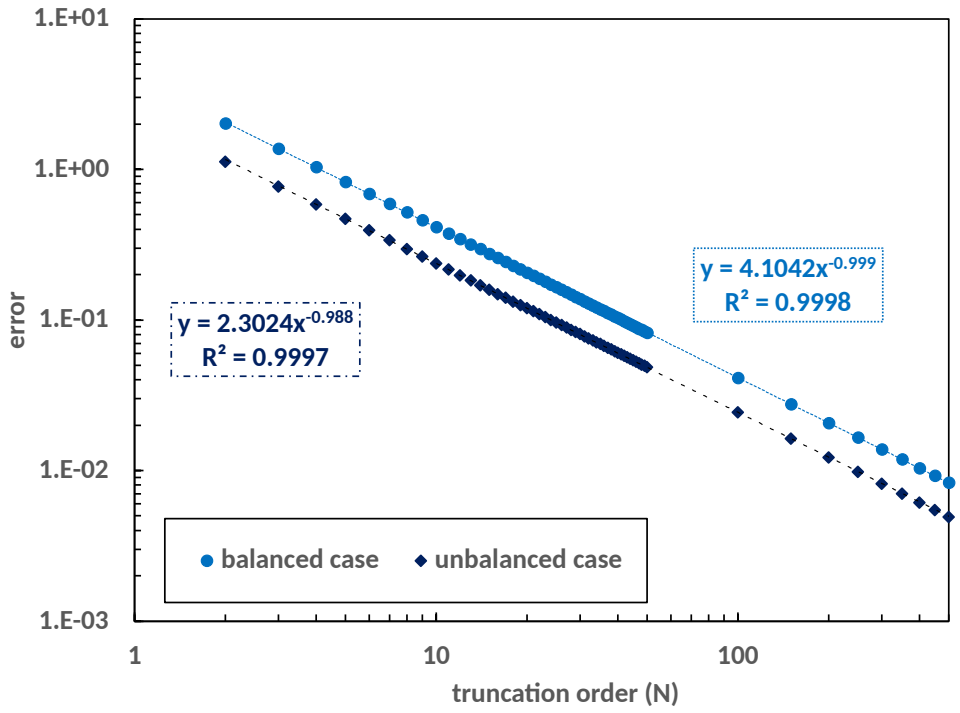

Figure 6: Error as function of the truncation order for both balanced and unbalanced cases

4.2.2. 1D-Beam model

For both balanced and unbalanced cases, as a function of the truncation order N, the variation of the error indicator as well as the absolute values of relative difference in interface displacement jumps in shear δ_u and in peel δ_v in $x = -L$ and $x = +L$ are provided in Fig. 8, Fig. 9 and Fig. 10 respectively. The same tendencies as for the 1D-bar model are observed. The absolute values of relative difference in displacement jumps are the same in $x = -L$ and in $x = +L$ for every truncation number N for the balanced case. Moreover, the error as well as the relative difference are decreasing functions of increasing truncation number N. The more N is elevated, the more the approximated stiffness matrix components and the interface displacements jumps tends to the reference ones. A convergence in around $\frac{1}{N}$ for the error indicator and displacement jumps in shear and in peel is then measured. Finally, relative differences in displacement jumps in shear and in peel around 1% are obtained for $N = 100$.

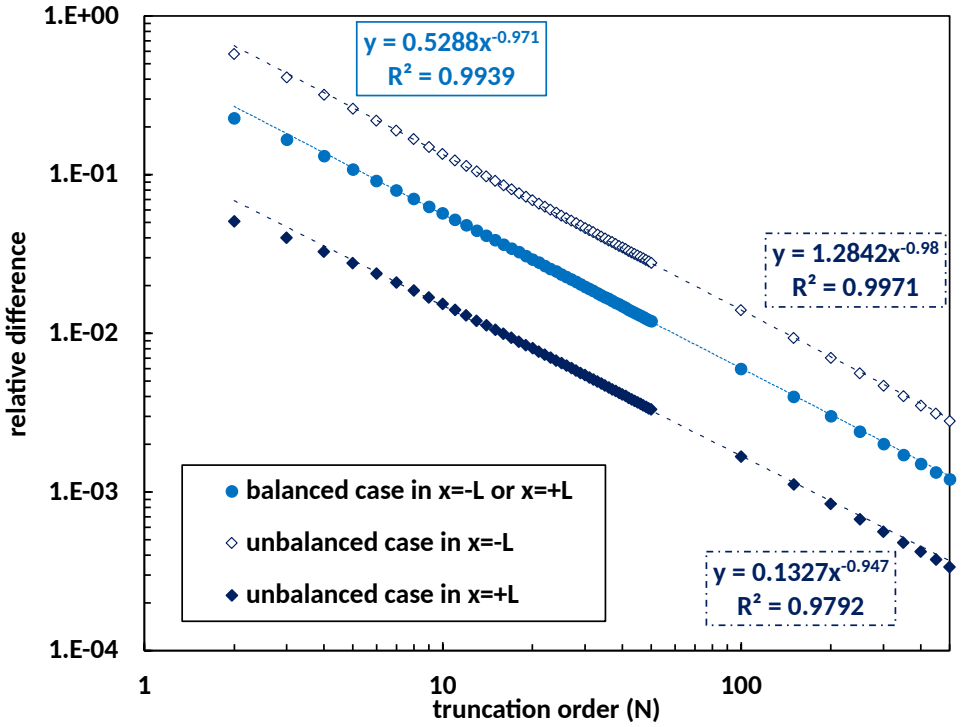

Figure 7: Relative difference in interface displacement jumps in shear at both overlap ends as function of the truncation order for both balanced and unbalanced cases

4.3. Comparison between FES and TEPS formulations

A formulation methodology of 1D-bar and 1D-beam ME stiffness matrices based on TEPS was presented by Ordonneau et al. and a Matlab code is available as a supplementary material of [28]. In the present paper, a new methodology based on TEPS for the formulation of these stiffness matrices are presented in addition of the FES formulation. The objective of the current section is to compare the FES and both TEPS formulation in terms of convergence. Only the balanced case is under consideration in this section. The results and associated conclusions are the same for the unbalanced case and are provided in Appendix A.

For the 1D-bar model, as a function of the truncation order N, the variation of the error indicator as well as the absolute values of relative difference in interface displacement jumps in shear δ_u in $x = -L$ are provided in Fig. 11 and Fig. 12 respectively. For the 1D-beam model, as a function of the truncation order N, the variation of the error indicator as well as the absolute values of relative difference in interface displacement jumps in shear δ_u and in peel δ_u in $x = -L$ are provided in Fig. 13, Fig. 14 and Fig. 15 respectively.

It is shown that, for the 3 series formulation, the error indicator and the relative difference in interface displacements jumps converge with increasing function for both 1D-bar and 1D-beam models. Moreover, for low truncation number N, the FES formulation appears to provide better or similar approximations as the TEPS formulation while, for higher truncation numbers, the TEPS formulations provide significantly closer approximations. Indeed, the convergence for TEPS formulations speeds up from $N = 10$ and lesser. For $N = 10$, the TEPS

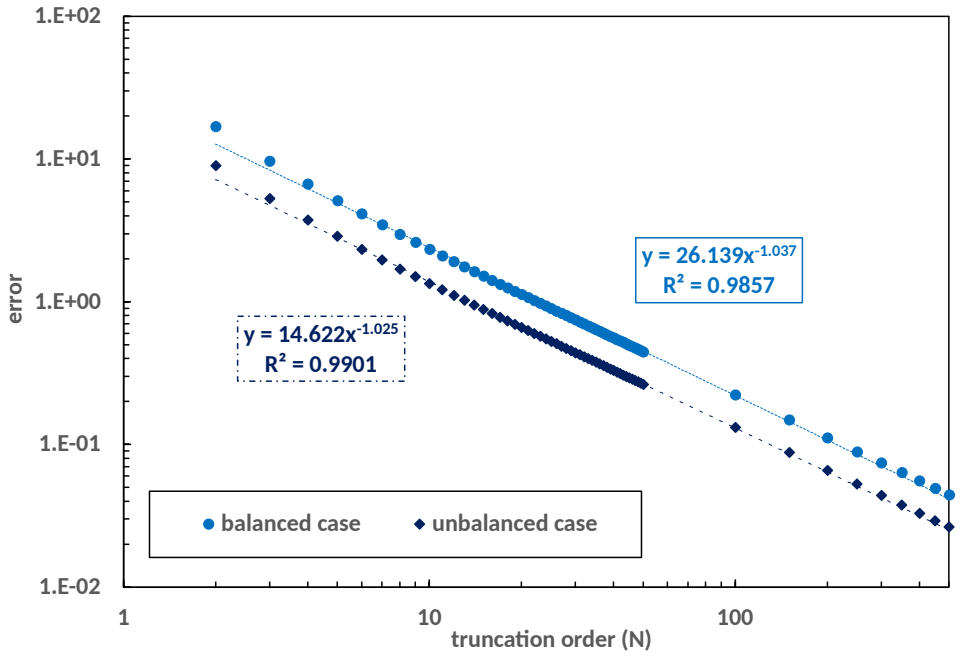

Figure 8: Error as function of the truncation order for both balanced and unbalanced cases

formulations provide relative difference 10 to 100 times lower than the FES formulation. Finally, for the 1D-bar model, not any differences in terms of convergence are shown between the TEPS formulation. For the 1D-beam model, the TEPS formulation by Ordonneau et al. [28] converge lightly quickly than the present TEPS formulation.

4.4. Remarks

The methodology presented in for the formulation of ME stiffness matrix using TEPS and FES as well as their implementation appear as validated for both 1D-bar and 1D-beam model. The stiffness matrix components and the interface displacement jumps converge to the reference ones. For a truncation order $N = 100$ ($N = 10$) relative differences in interface displacement jumps around 1% are obtained with FES (TEPS) formulation. The convergence rate associated with the FES formulation is regular and depend on $\frac{1}{N}$. On the contrary, the TEPS formulation convergence rate is characterized by a significant speed up at low truncation numbers. The present TEPS formulation present similar or lesser convergence as the one presented by Ordonneau et al. [28]. Nevertheless, the methodology for the present TEPS formulation is straight forward since it considers the first order differential equations deduced from the simplifying hypotheses. Contrary to the one presented by Ordonneau et al., not any algebraic manipulations are required. Finally, elements on computation cost could be interesting. However, computational times are dependent on the implementation quality and implementation platform used. As a result, instead of a quantitative assessment, a qualitative assessment is preferred based on the coupling matrix$_{DME}$, the inversion of which is necessary for both TEPS and FES formulation. The size of DME is equal to $P(N+1)$ and $P(2N+1)$ for TEPS and FES formulations respectively, so that the TEPS formulation

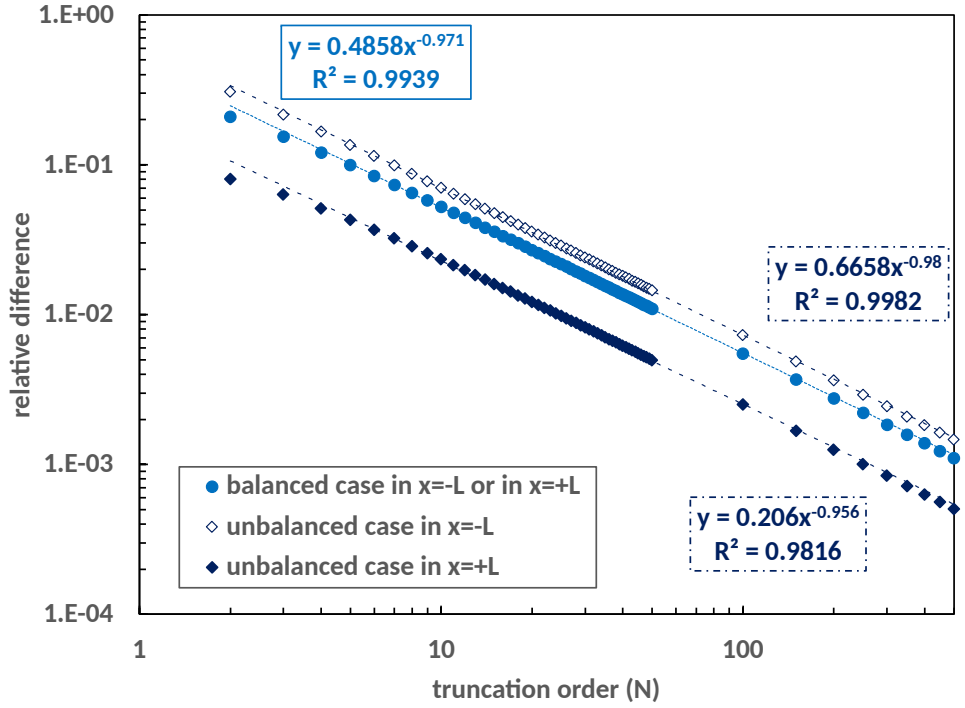

Figure 9: Relative difference in interface displacement jumps in shear at both overlap ends as function of the truncation order for both balanced and unbalanced cases

qualitatively appears less costly.

4.5. Application on the single-lap bonded joint test case

4.5.1. Overview

The computation of adhesive stresses by the ME modelling has already been (i) validated with respect to classical theories (e.g. [20, 32]) by demonstrating that the same hypotheses lead to the same results and (ii) assessed with respect to refined FE methods (e.g. [21, 28]) on various types of bonded joints, eventually including nonlinear adhesive material behaviors. In this section, the adhesive shear and peel stress distributions along the overlap of the single-lap bonded joint are considered. The single-lap bonded joint is supposed (i) made with adherends having the same elastic linear isotropic homogeneous materials, (ii) in-plane loaded by a tensile force of $f = 5$ kN and simply supported at both extremities (see Figure 1). Under these hypotheses the classical theory of Goland and Reissner [14] can be applied. The geometrical parameters are given in Table 1. Moreover, the length outside the overlap of both adherends is equal to $l_1 = l_2 = 50$ mm. The material parameters for the adhesive are provided in Table 2. The Young's modulus and Poisson's ratio are supposed equal to 70 GPa and 0.35 respectively. 1D-beam ME models and a 2D FE plane strain model of this joint are built. For the ME model, the computation is made considering for the overlap either the reference stiffness matrix (see Section 4.1) or the stiffness matrix formulated using the FES. The objective is to compare the adhesive stress distribution obtained by the different approaches.

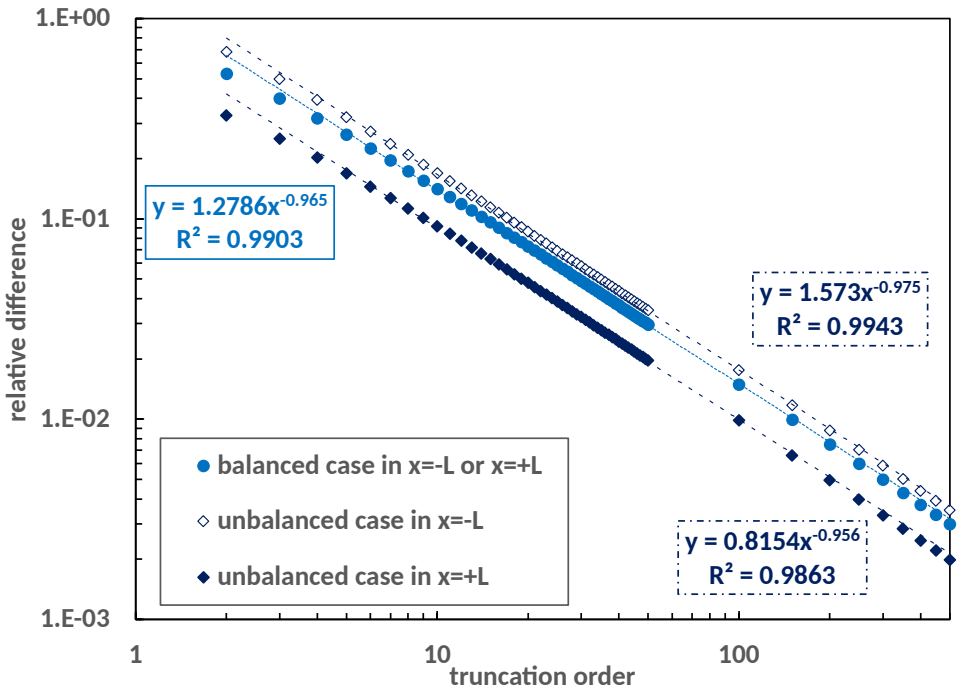

Figure 10: Relative difference in interface displacement jumps in peel at both overlap ends as function of the truncation order for both balanced and unbalanced cases

4.5.2. ME model

The ME model of the single-lap bonded joint (Figure 1) is built with one macro-elements representing for the adherends and the adhesive layer along the overlap and two beam elements representing the adherends outside the overlap [11]. The structural stiffness matrix K_s is then assembled from the elementary ME stiffness matrix K_{ME} and the beam element stiffness matrix $K_{beam,i}$ for the adherend i where:

$$K_{beam,i} = \begin{pmatrix} A_i/l_i & -A_i/l_i & 0 & 0 & 0 & 0 \\ -A_i/l_i & A_i/l_i & 0 & 0 & 0 & 0 \\ 0 & 0 & 12\frac{D_i}{l_i^3} & -12\frac{D_i}{l_i^3} & 6\frac{D_i}{l_i^2} & 6\frac{D_i}{l_i^2} \\ 0 & 0 & -12\frac{D_i}{l_i^3} & 12\frac{D_i}{l_i^3} & -6\frac{D_i}{l_i^2} & -6\frac{D_i}{l_i^2} \\ 0 & 0 & 6\frac{D_i}{l_i^2} & -6\frac{D_i}{l_i^2} & 4\frac{D_i}{l_i} & 2\frac{D_i}{l_i} \\ 0 & 0 & 6\frac{D_i}{l_i^2} & -6\frac{D_i}{l_i^2} & 2\frac{D_i}{l_i} & 4\frac{D_i}{l_i} \end{pmatrix} \tag{84}$$

A total of 6 nodes is then involved, each node having 3 degrees of freedom. After the prescription of concerned displacements to ensure a simply support, a total of 15 degrees of freedom is obtained. When considering the ME stiffness matrix K_{ME} based on FES formulation, the ME model depends on the truncation order N. Here, 4 truncation orders are selected: $N = 2$, $N = 5$, $N = 50$ and $N = 500$. The minimization of the potential energy leads to the linear system $F_s = K_s U_s$ where U_s is the unknown nodal displacement vector and F_s the nodal displacement vector depending on the applied tensile load f. Finally, to

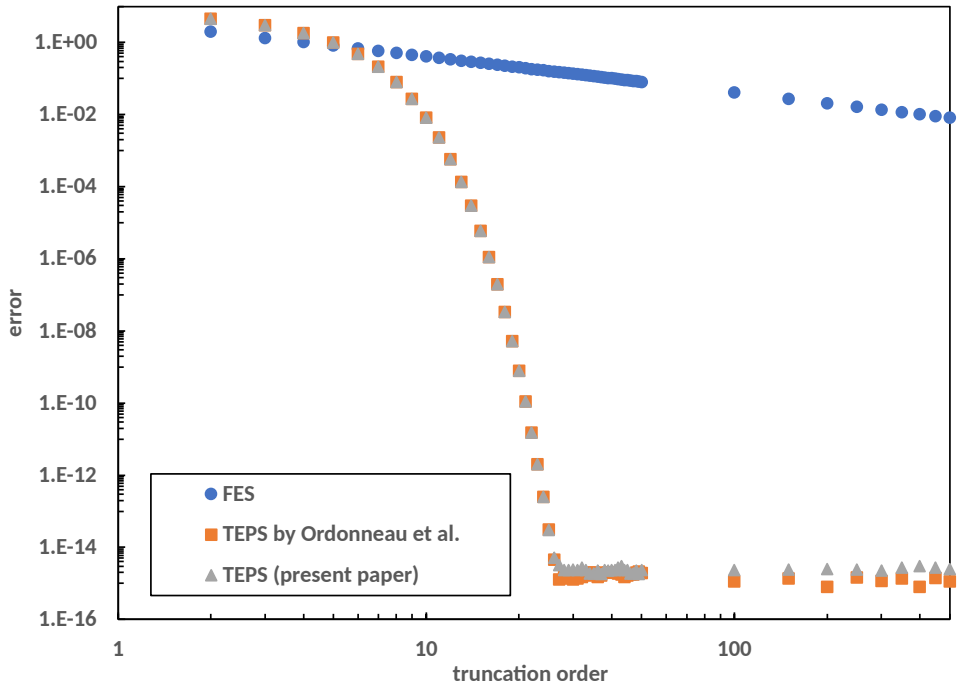

Figure 11: Error as function of the truncation order for the balanced case

consider the geometrically nonlinearity in terms of defection due to eccentricity of the load path, the lengths outside the overlap l_i are modified to get the bending moment and shear force at overlap ends such as predicted by Goland and Reissner ([11, 20]).

4.5.3. FE model

The 2D plane strain FE model of the single-lap bonded joint in Figure 1 is developed using the commercial FE software SAMCEF v21.1 (SIEMENS). The geometry as well as the material laws and parameters are the same as described previously. The adherends are meshed with linear 4-node elements under plane strain assumption with 2 degrees of freedom per node and normal Gaussian integration. The mesh strategy consists in refining the mesh in the areas subjected to high stress gradients: both ends of the bonded overlap. Moreover, the mesh of the FE model is designed to be driven by the number of elements in the adhesive layer at both overlap ends. At each of both extremities of the overlap and along a length of 4 mm, the adhesive is regularly meshed with elements, the aspect ratio of which is one. Along the rest of the overlap, the mesh is distributed towards the center of the overlap to reduce the size of the FE model (Fig. 16). At the interface between each adherend and the adhesive, kinematics bonding condition at coincident nodes is applied, meaning that a transition ratio equal to 1 is considered. To reduce the size of the FE model, the mesh is then distributed in the adherend thickness and along the length outside of the overlap. The prescription of displacements related to simply support conditions and the applied tensile force f are introduced by constraining 2 additional nodes linked to both joint extremities with rigid body elements (Figure 1 and Figure 16). Two computation cases are considered:

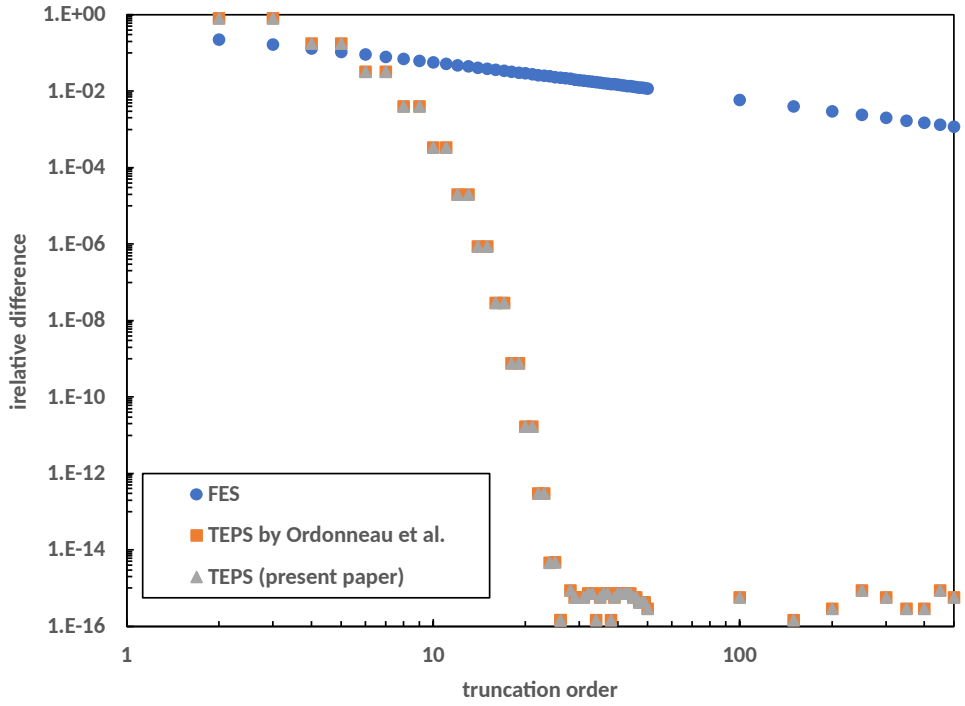

Figure 12: Relative difference in interface displacement jumps in shear in $x = -L$ as function of the truncation order for the balanced case

geometrically linear and geometrically nonlinear. The same iterative resolution based on the Newton Raphson scheme is then employed for both previous computation cases. The adhesive stresses measured are Cauchy stresses extrapolated at nodes and averaged with neighboring elements. The adhesive stresses are measured along the overlap at the middle of the adhesive thickness.

To justify the mesh convergence, four different numbers of elements in the adhesive thickness are tested: 2, 4, 8 and 12 elements leading to densities of 10, 20, 40 and 60 elements per mm in the adhesive thickness – since $e_a = 0.2$ mm – respectively. The adhesive peak stresses in shear and in peel for a density of 60 elements per mm are taken as a references. The ratio between the adhesive peak stress in shear and in peel for a given number of elements in the adhesive thickness with the related reference adhesive peak stress in shear and in peel is provided as a function of the meh density in Figure 17. It is shown that with 12 elements in the adhesive thickness, the FE model can be regarded as converged.

4.5.4. Comparison

The adhesive shear and peel stress distributions along the overlap provided by the ME models and FE model are given in Figure 18 and Figure 19 for geometrically linear and nonlinear assumptions respectively. Moreover, the adhesive stress distribution by Goland and Reissner [14] are added in Figure 19. The adhesive stress distributions predicted by the ME models based K_{ME} based on FES formulation converge when the truncation order N is increased as expected. The ME model with K_{ME} based on FES formulation at $N = 500$ provides

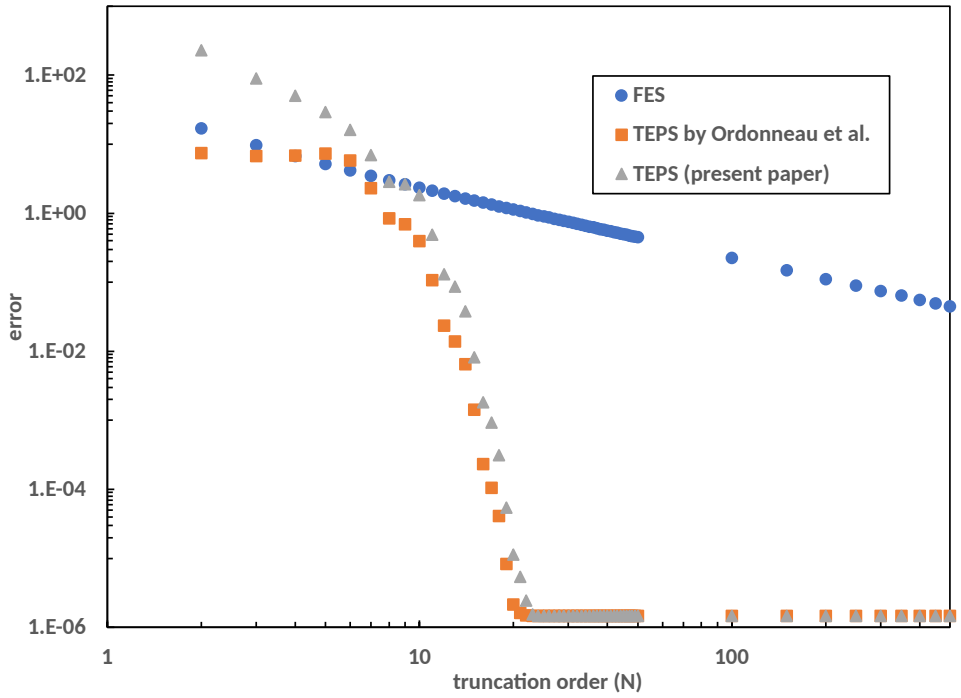

Figure 13: Error as function of the truncation order for the balanced case

maximal adhesive shear and peel peak stresses relatively different from the ones predicted by ME model with the reference K_{ME} stiffness matrix of -0.12% and -0.30% respectively for both geometrically linear and nonlinear assumptions. Besides, in both geometrically linear and nonlinear assumptions, the adhesive distributions provided by the ME and FE models are in very close agreement. The differences appear at both overlap ends. As the ME models are based on a simple beam on elastic foundation approach, they are not able to capture at free ends (i) the tendency of the adhesive shear stress to drop to zero and (ii) the induced brutal decrease of the peel stress, contrary to the converged FE model. Small differences in terms of peak stresses can then be measured. The same conclusions arise when considering the adhesive stress distributions given by the Goland and Reissner theory instead of those by the ME models. Another source of difference is due to the various set hypotheses of models. The ME model are 1D-beam models involving true Young's modulus while the FE model is under plane strain assumption resulting in effective Young's modulus. This the same for the theory by Goland and Reissner: the shear stress is assessed through the adherend true Young's modulus while the peel stress makes appear the adherend effective Young's modulus. That is why, in particular, the adhesive shear stress distribution given by the converged ME model tends to the Goland and Reissner one contrary to the peel stress distribution (see Figure 19).

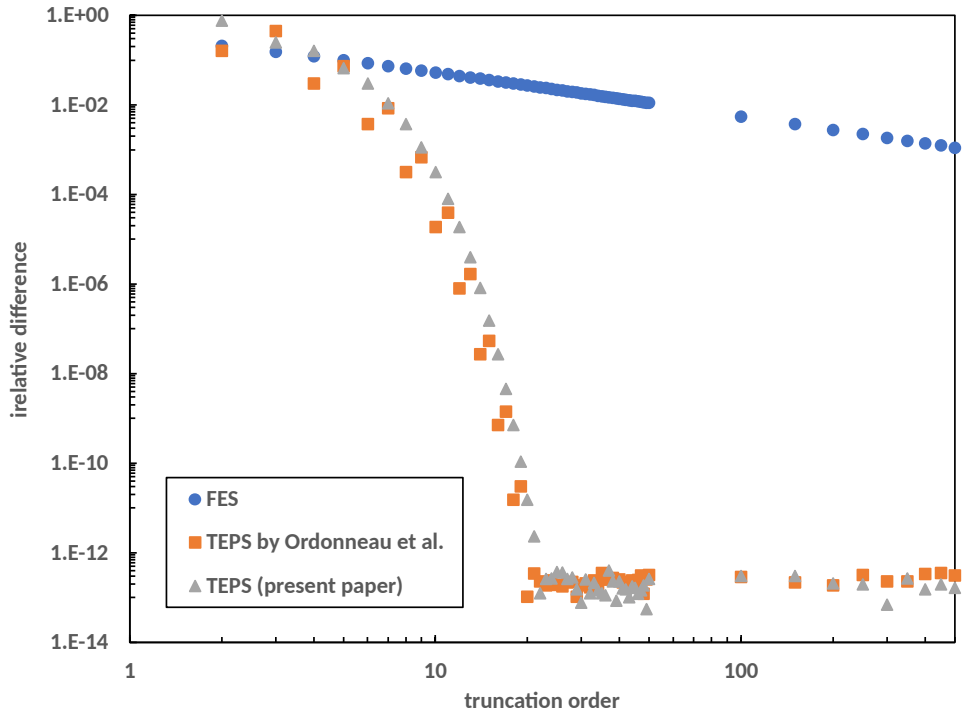

Figure 14: Relative difference in interface displacement jumps in shear in $x = -L$ as function of the truncation order for the balanced case

5. Conclusion and perspectives

In the frame of the simplified stress analysis of adhesively bonded single-lap joints, it is common to model the adherends as beams or cylindrically bending plates and the adhesive layer as a bed of springs. Even under these simplifications, the expressions for the mechanical fields in closed-for manner is not always possible, all the more when the models are enriched (graduation of properties, variation of constitutive equations, boundary conditions). Semi-analytical approaches associated with dedicated resolution schemes, such as the macro-element modelling able to represent for an entire length bonded overlap with only one 4-nodes brick, become then necessary. In this paper, the formulation of ME stiffness matrix of an entire adhesively bonded joint is approximated using Taylor expansion poser series and of Fourier expansion series. A methodology associated with each of both previous expansion series is presented and implemented. Both methodologies are validated by comparing the stiffness matrix components term by term and the interface displacement jumps with the results from exact formulation. In addition, the formulation based on Taylor expansion power series offer a significantly convergence rate associated with an expected lesser computation cost. Nevertheless, the use of FES does not make disappear series terms so that it is not necessary to look for additional equations. In the frame of 1D-bar or 1D-beam models, the finding of additional equations is obvious. But the finding of additional equations prevented Ordonneau [29] from the formulation of the macro-element stiffness matrix of an entire overlap made of 2D plates bonded by a bed of springs – associated with the peel and both shear

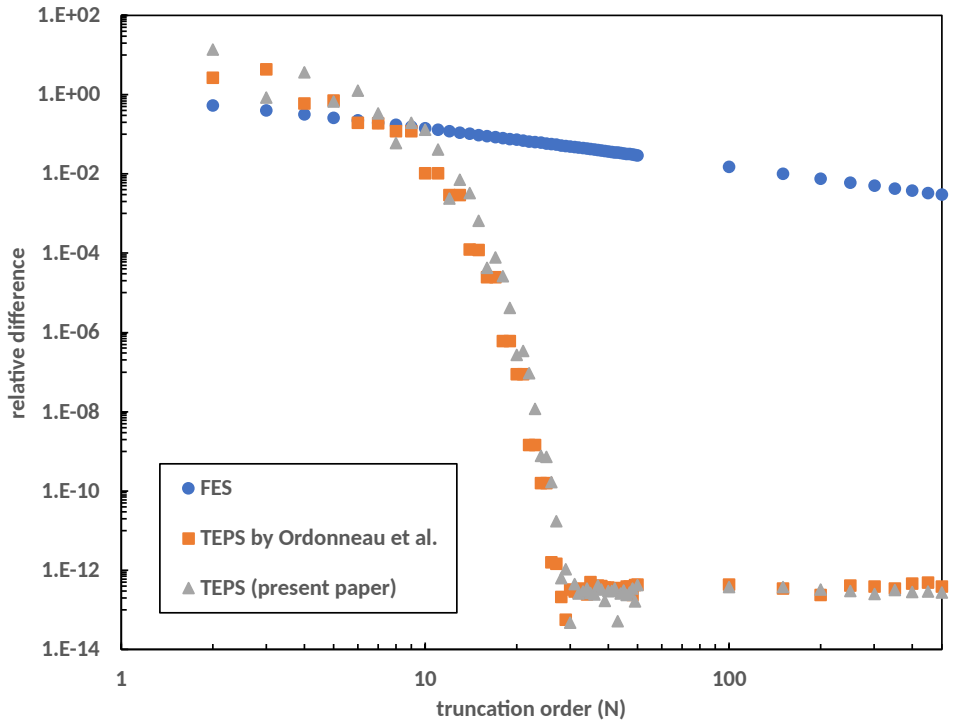

Figure 15: Relative difference in interface displacement jumps in peel in $x = -L$ as function of the truncation order for the balanced case

displacement jumps. The use of FES could then be tested as a future work.

Conflict of interest

Michel Salaün, Eric Paroissien, Sébastien Schwartz, Tuan-Long Vu, Valeria De Angelis, Maxime Luyat and Benjamin Ordonneau declare that they have no conflict of interest.

Acknowledgements

Yves Caumel (1947-2019) gave the opportunity to Michel Salaün to teach Fourier series, among many other topics, to engineering students, many years ago. At this time, he was not thinking he could use it in a research paper... Today, Michel Salaün wishes to dedicate this paper to Yves Caumel, a great professor and a great friend. *In memoriam*.

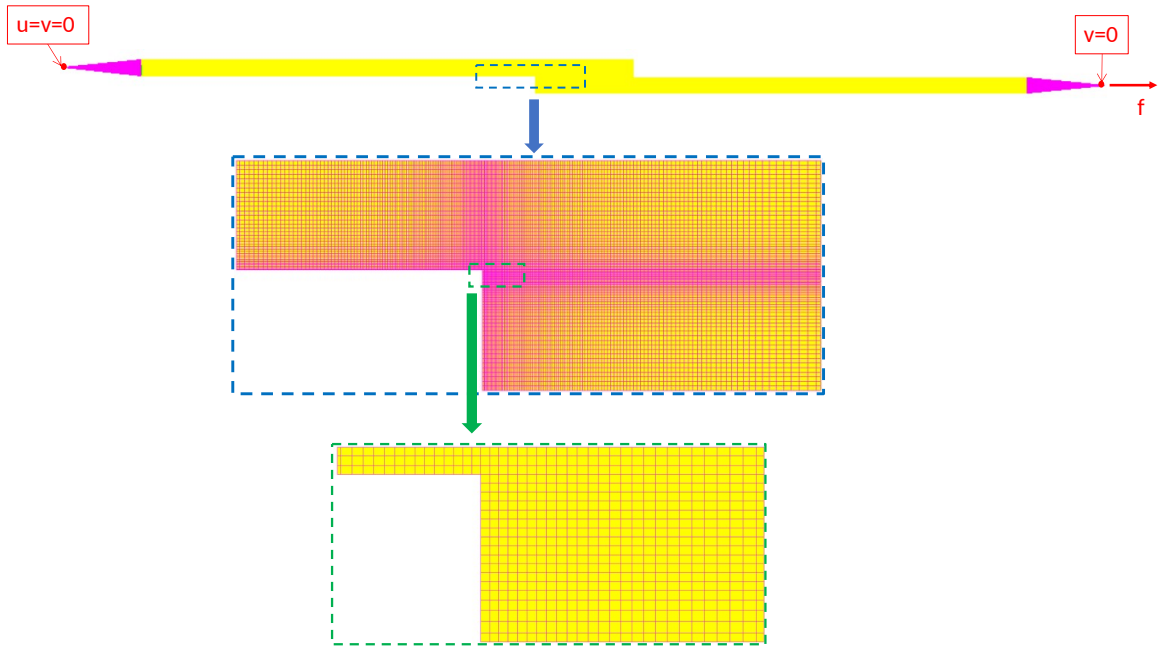

Figure 16: Mesh of the FE model and boundary conditions.

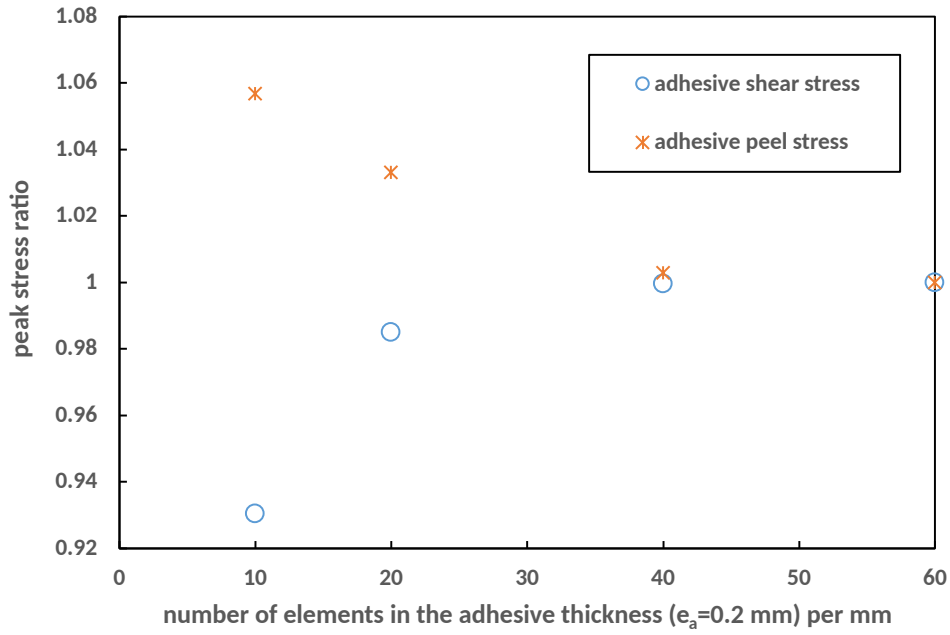

Figure 17: Ratio between the adhesive peak stress in shear and in peel for a given number of element in the adhesive thickness with the related reference adhesive peak stress is provides as a function of the meh density.

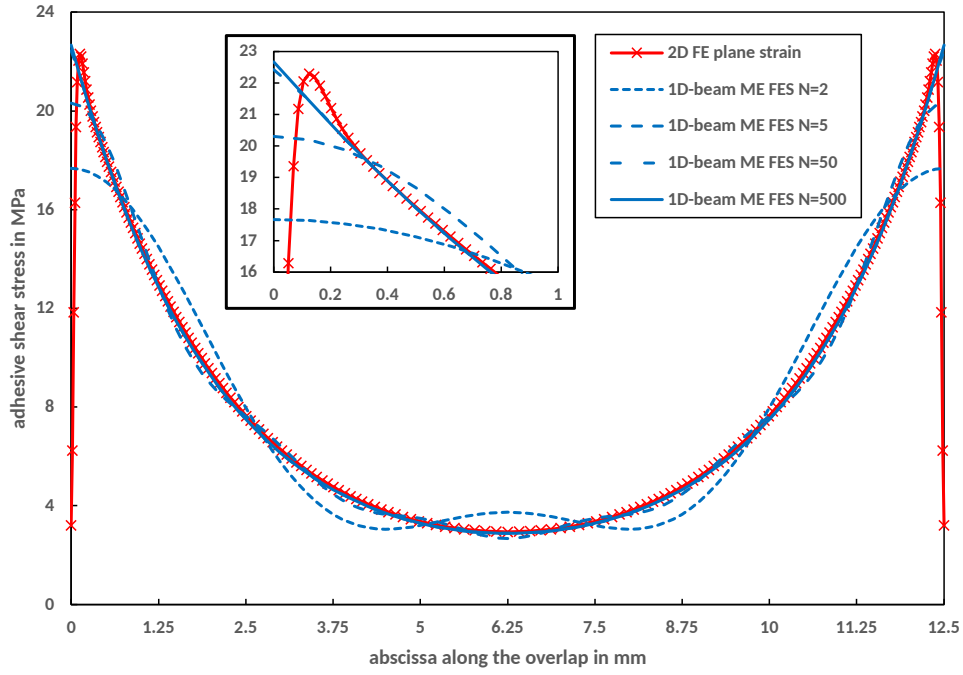

(a) Shear stresses

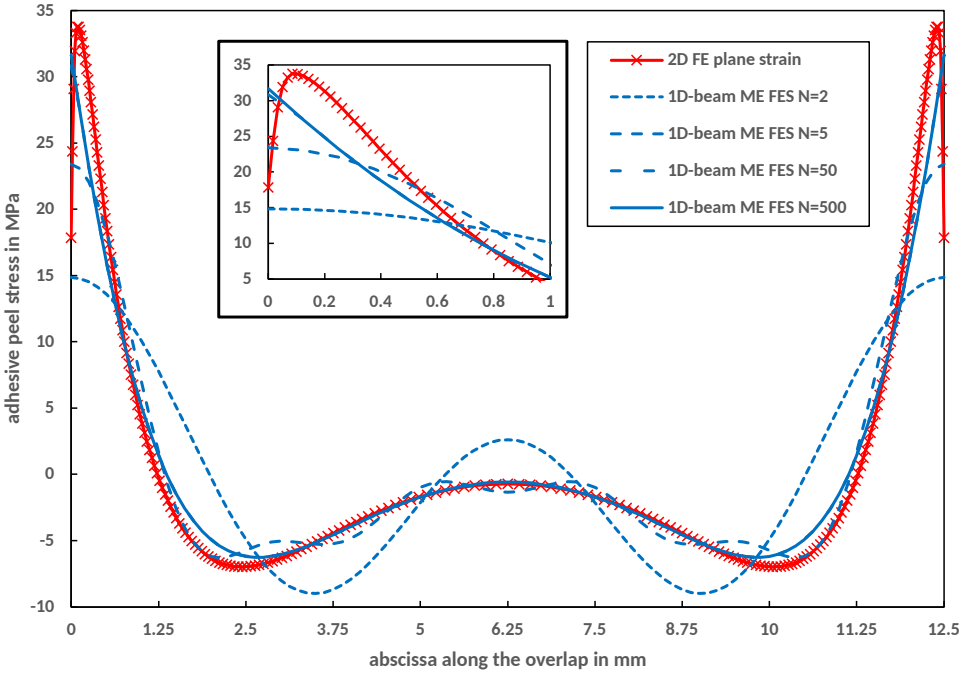

(b) Peel stresses

Figure 18: Distribution along the overlap of the adhesive shear stress (a) and peel stress (b) provided by the ME models and the FE model under geometrically linear assumption. A focus on the stress distribution along the first millimeter is added.

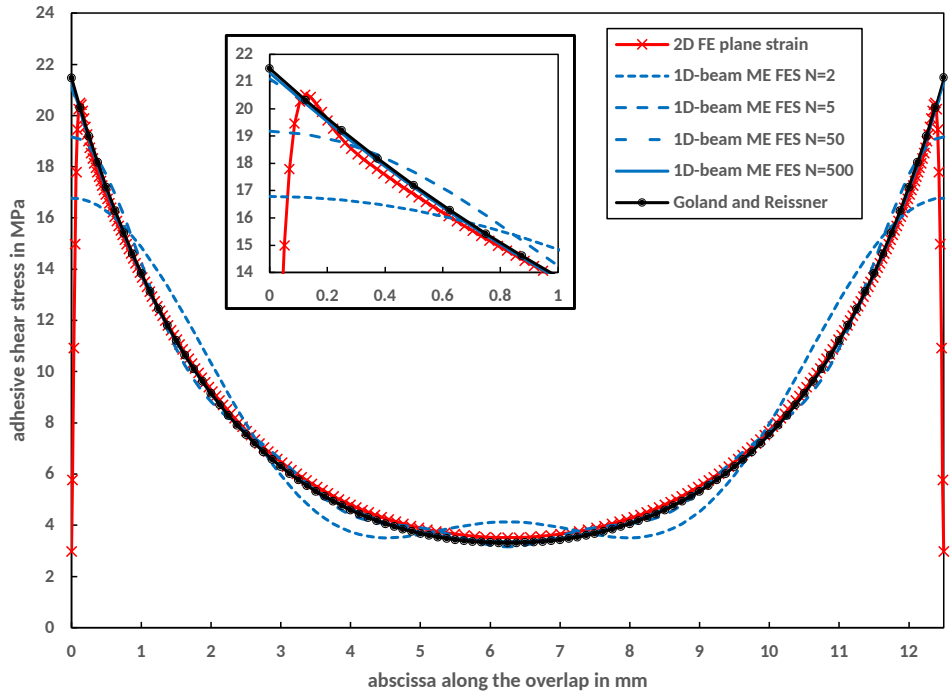

(a) Shear stresses

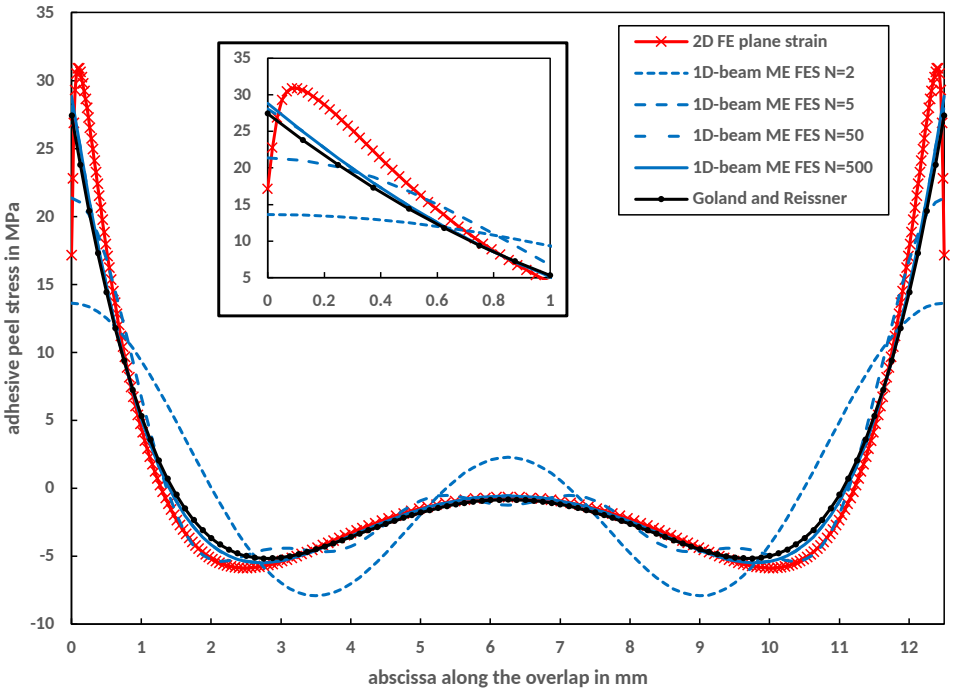

(b) Peel stresses

Figure 19: Distribution along the overlap of the adhesive shear stress (a) and peel stress (b) provided by the ME models and the FE model under geometrically nonlinear assumption and by Goland and Reissner theory. A focus on the stress distribution along the first millimeter is added.

Appendix A. Appendix

The results for the comparison of FES and both TEPS formulation for the unbalanced case are given in this appendix. The relative difference in interface displacement jumps is given in $x = -L$ only since those in $x = +L$ are similar.
For the 1D-bar model, as a function of the truncation order N, the variation of the error indicator as well as the absolute values of relative difference in interface displacement jumps in shear δ_u in $x = -L$ are provided in Fig. A.1 and Fig. A.2 respectively.

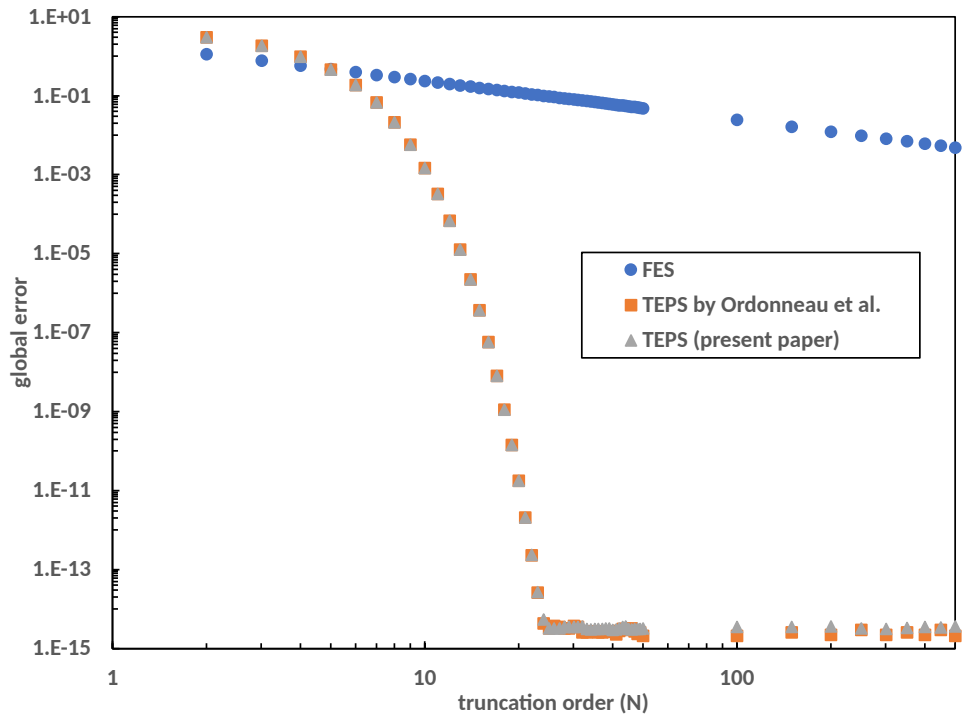

Figure A.1: Error as function of the truncation order (in log scale) for the unbalanced case

For the 1D-beam model, as a function of the truncation order N, the variation of the error indicator as well as the absolute values of relative difference in interface displacement jumps in shear δ_u and in peel δ_v in $x = -L$ are provided in Fig. A.3, Fig. A.2 and Fig. A.5 respectively.

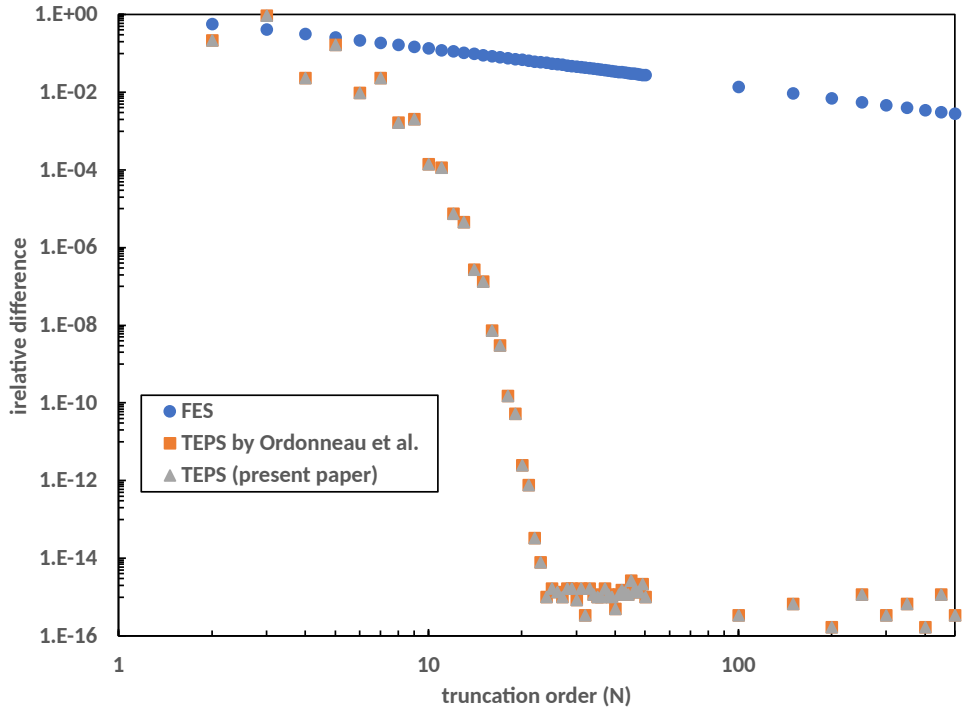

Figure A.2: Relative difference in interface displacement jumps in shear in $x = -L$ as function of the truncation order (in log scale) for the unbalanced case

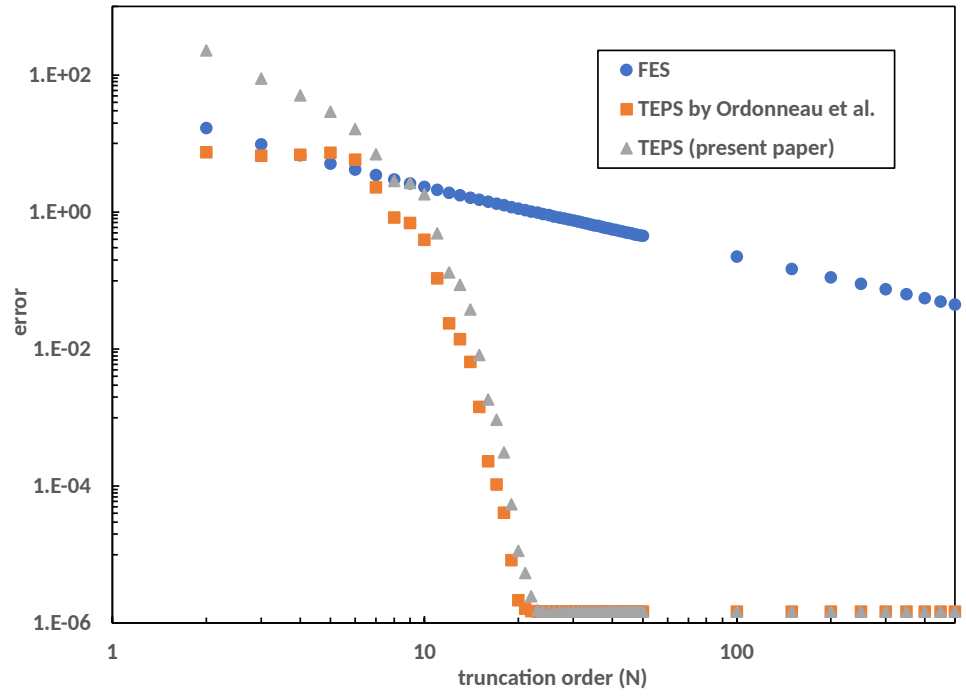

Figure A.3: Error as function of the truncation order (in log scale) for the unbalanced case

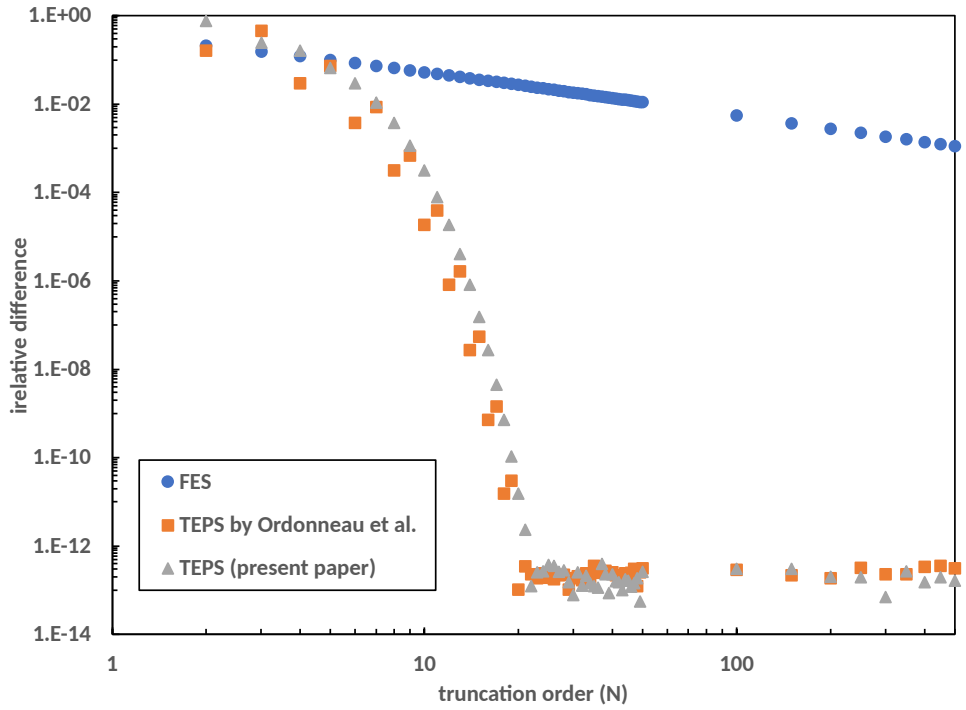

Figure A.4: Relative difference in interface displacement jumps in shear in $x = -L$ as function of the truncation order (in log scale) for the unbalanced case

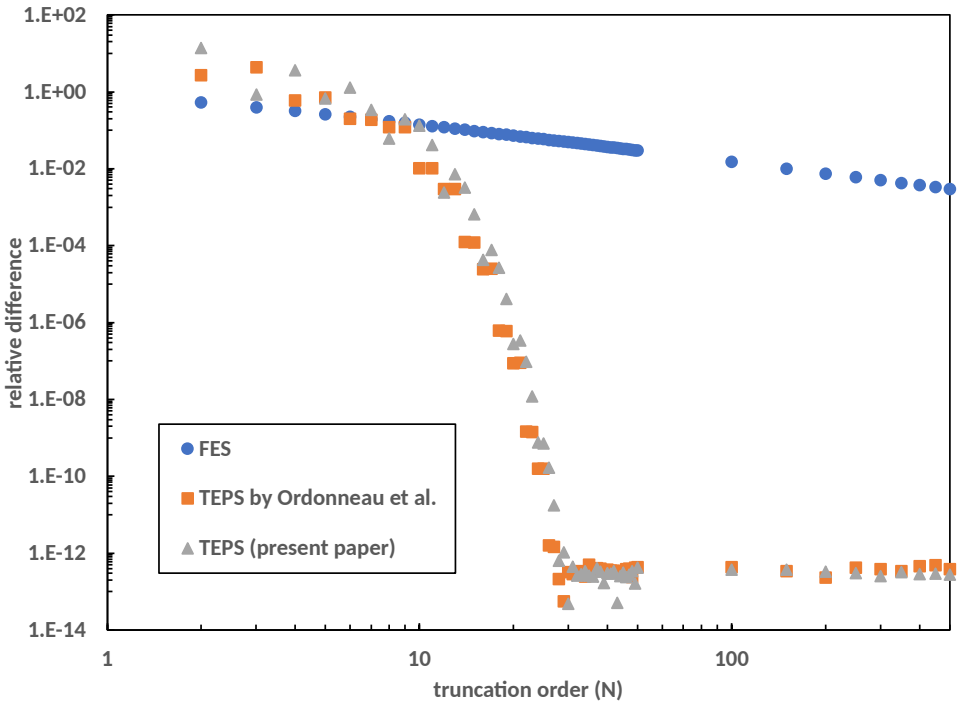

Figure A.5: Relative difference in interface displacement jumps in peel in $x = -L$ as function of the truncation order (in log scale) for the unbalanced case

References

[1] G. R. Wooley, D. R. Carver, Stress concentration factors for bonded lap joint, Journal of Aircraft 8 (1971) 817–820. doi:10.2514/3.44305.

[2] J. A. Harris, R. D. Adams, Strength prediction of bonded single lap joints by non-linear finite element methods, International Journal of Adhesion and Adhesives 4 (2) (1984) 65–78. doi:10.1016/0143-7496(84)90103-9.

[3] X. He, A review of finite element analysis of adhesively bonded joints, International Journal of Adhesion and Adhesives 31 (4) (2011) 248–264. doi:10.1016/j.ijadhadh.2011.01.006.

[4] S. Budhe, M. D. Banea, S. de Barros, L. F. M. da Silva, An updated review of adhesively bonded joints in composite materials, International Journal of Adhesion and Adhesives 72 (2017) 30–42. doi:10.1016/j.ijadhadh.2016.10.010.

[5] L. D. C. Ramalho, R. D. S. G. Campilho, J. Belinha, L. F. M. da Silva, Static strength prediction of adhesive joints: A review, International Journal of Adhesion and Adhesives 96 (2020) 102451. doi:10.1016/j.ijadhadh.2019.102451.

[6] K. Tserpes, A. Barroso-Caro, P. A. Carraro, V. C. Beber, I. Floros, W. Gamon, M. Kozłowski, F. Santandrea, M. Shahverdi, D. Skejić, C. Bedon, V. Rajčić, A review on failure theories and simulation models for adhesive joints, The Journal of Adhesion (2021) 1–61doi:10.1080/00218464.2021.1941903.

[7] J. W. van Ingen, A. Vlot, Stress analysis of adhesively bonded single lap joints, Tech. Rep. LR-740, Delft University of Technology (1993).

[8] L. F. M. da Silva, P. J. C. das Neves, R. D. Adams, J. K. Spelt, Analytical models of adhesively bonded joints – Part I: Literature survey, International Journal of Adhesion and Adhesives 29 (2009) 319–330. doi:10.1016/j.ijadhadh.2008.06.005.

[9] L. F. M. da Silva, P. J. C. das Neves, R. D. Adams, J. K. Spelt, Analytical models of adhesively bonded joints – Part II: Comparative study, International Journal of Adhesion and Adhesives 29 (2009) 331–341. doi:10.1016/j.ijadhadh.2008.06.007.

[10] E. H. Wong, J. Liu, Interface and interconnection stresses in electronic assemblies – A critical review of analytical solutions, Microelectronics Reliability 79 (2017) 206–220. doi:10.1016/j.microrel.2017.03.010.

[11] E. Paroissien, F. Lachaud, S. Schwartz, Modelling load transfer in single-lap adhesively bonded and hybrid (bolted / bonded) joints, Progress in Aerospace Sciences 130 (2022) 100811. doi:10.1016/j.paerosci.2022.100811.

[12] I. Arnovljevic, Das verteilungsgesetz der tiefspannungen in axial beanspruchten verbundstaben, Z. F. Archund-Ing-Wesen 55 (1909) 415–418.

[13] O. Volkersen, Die nietkraftverteilung in zugbeanspruchten nietverbindungen mit konstanten laschenquerschnitten, Luftfahrforschung 15 (24) (1938) 41–47.

[14] M. Goland, E. Reissner, The stresses in cemented joint, Journal of Applied Mechanics 11 (1) (1944) A17–A27. doi:10.1115/1.4009336.

[15] F. Mortensen, O. T. Thomsen, Simplified linear and non-linear analysis of stepped and scarfed adhesive-bonded lap-joints between composite laminates, Composite Structures 38 (1-4) (1997) 281–294. doi:10.1016/S0263-8223(97)00063-9.

[16] F. Mortensen, Development of tools for engineering analysis and design of high-performance FRP-composite structural elements, Ph.D. thesis, Aalborg University (1998).

[17] F. Mortensen, O. T. Thomsen, Analysis of adhesive bonded joints: A unified approach, Composites Science and Technology 62 (2002) 1011–1031. doi:10.1016/S0266-3538(02)00030-1.

[18] F. Mortensen, O. T. Thomsen, Coupling effects in adhesive bonded joints, Composite Structures 56 (2002) 165–174. doi:10.1016/S0266-3538(02)00030-1.

[19] A. Kalnins, Analysis of shell of revolutions subjected to symmetrical and non-symmetrical loads, Journal of Applied Mechanics 31 (1964) 1355–1365. doi:10.1121/1.1919208.

[20] E. Paroissien, M. Sartor, J. Huet, F. Lachaud, Analytical two-dimensional model of a hybrid (bolted/bonded) single-lap joint, Journal of Aircraft 44 (2) (2007) 573–582. doi:10.2514/1.24452.

[21] E. Paroissien, F. Lachaud, S. Schwartz, A. da Veiga, P. Barrière, Simplified stress analysis of hybrid (bolted/bonded) joints, International Journal of Adhesion and Adhesives 77 (2017) 183–197. doi:10.1016/j.ijadhadh.2017.05.003.

[22] G. Lélias, E. Paroissien, F. Lachaud, J. Morlier, S. Schwartz, C. Gavoille, An extended semi-analytical formulation for fast and reliable stress analysis of adhesively bonded joints, International Journal of Solids and Structures 62 (2015) 18–39. doi:10.1016/j.ijsolstr.2014.12.027.

[23] F. Lachaud, E. Paroissien, L. Michel, Validation of a simplified analysis for the simulation of delamination of CFRP composite laminated materials under pure mode I, Composite Structures 237 (2020) 111897. doi:10.1016/j.compstruct.2020.111897.

[24] E. Paroissien, L. F. M. da Silva, F. Lachaud, Simplified stress analysis of functionally graded single-lap joints subjected to combined thermal and mechanical loads, Composite Structures 203 (2018) 85–100. doi:10.1016/j.compstruct.2018.07.015.

[25] K. Sekmen, E. Paroissien, F. Lachaud, Simplified stress analysis of multilayered adhesively bonded structures, International Journal of Adhesion and Adhesives 97 (2020) 102497. doi:10.1016/j.ijadhadh.2019.102497.

[26] S. Schwartz, E. Paroissien, F. Lachaud, General formulation of macro-elements for the simulation of multi-layered bonded structures, The Journal of Adhesion 96 (6) (2020) 602–632. doi:10.1080/00218464.2019.16224207.

[27] V. Torrelli, E. Paroissien, Simplified stress analysis of multilayered bonded structure under 1d-bar kinematics, Composite Structures 251 (2020) 112641. doi:10.1016/j.compstruct.2020.112641.

[28] B. Ordonneau, E. Paroissien, M. Salaün, J. Malrieu, A. Guigue, S. Schwartz, A methodology for the computation of the macro-element stiffness matrix for the stress analysis of a lap joint with functionally graded adhesive properties, International Journal of Adhesion and Adhesives 97 (2020) 102505. doi:10.1016/j.ijadhadh.2019.102505.

[29] B. Ordonneau, E. Paroissien, M. Salaün, A. Benitez-Martin, S. Schwartz, J. Malrieu, A. Guigue, A simplified modal analysis of a single lap bonded joint using the macro-element technique, International Journal of Solids and Structures 249 (2022) 111631. doi:10.1016/j.ijsolstr.2022.111631.

[30] B. Ordonneau, Méthodologie pour la simulation rapide et fiable de structures collées multi-couches sous sollicitation dynamique, Ph.D. thesis, Université de Toulouse (2021).

[31] Y. Caumel, Cours d'analyse fonctionnelle et complexe, Cépaduès, 2003.

[32] E. Paroissien, M. Sartor, J. Huet, Hybrid (Bolted/Bonded) Joints Applied to Aeronautic Parts: Analytical One-Dimensional Models of a Single-Lap Joint, in: S. Tichkiewitch, M. Tollenaere, P. Ray (Eds.), Advances in Integrated Design and Manufacturing in Mechanical Engineering II, Springer Netherlands, Dordrecht, 2007, pp. 95–110. doi:10.1007/978-1-4020-6761-7_7.

[33] S. Cheng, D. Chen, Y. Shi, , Journal of Engineering Mechanics 117 (3) (1991) 605–623. doi:10.1061/(ASCE)0733-9399(1991)117:3(605).